
Sensitivity of EFITs to the Form of the MSE Fitting Function

M.A. Makowski, S. Allen, R. Ellis,
R. Geer, J. Jayakumar, J. Moller, B. Rice

Poster RP1-020

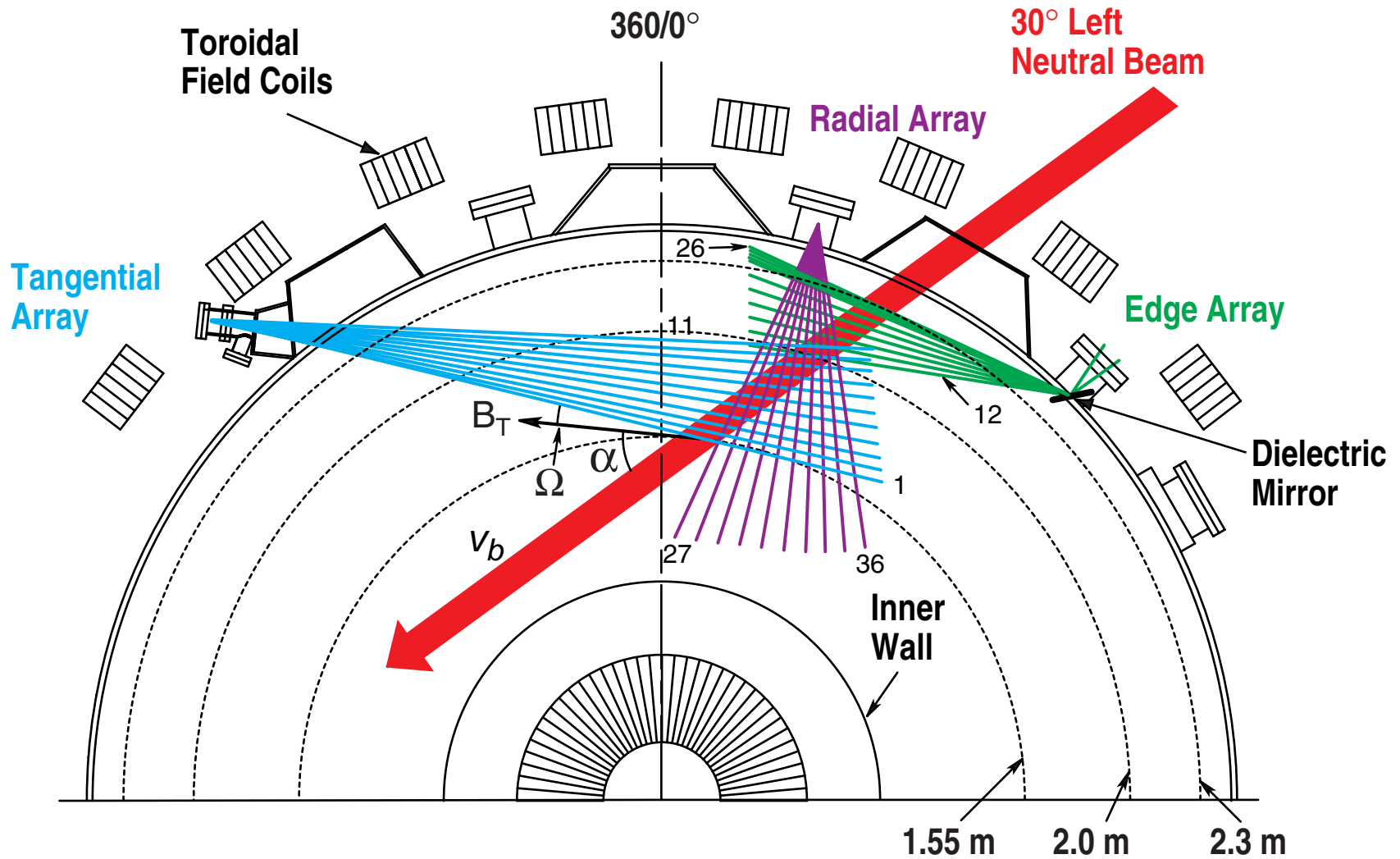


Issues and Motivation

- The form of the fitting function is found to have an effect on the measured pitch angles
- While relatively small ($0.2^\circ - 0.4^\circ$), the differences can influence:
 - the location of the magnetic axis
 - the magnitude of E_r
 - the boundary of the plasma



MSE Layout on DIII-D



Fitting Functions Differ Slightly in Form

- Currently use the “tangent-slope” form

$$\frac{S_m}{C_m} = G \tan[2(\sigma \cdot \gamma + \varphi)]$$

- However, the “tangent-offset” form is better justified

$$\frac{S_m}{C_m} = G \tan[2(\gamma + \varphi)] + G_0$$

- In the limit that $\sigma = 1$ and $G_0 = 0$, the two forms coincide



$\sigma=1$ is the Only Justified Value

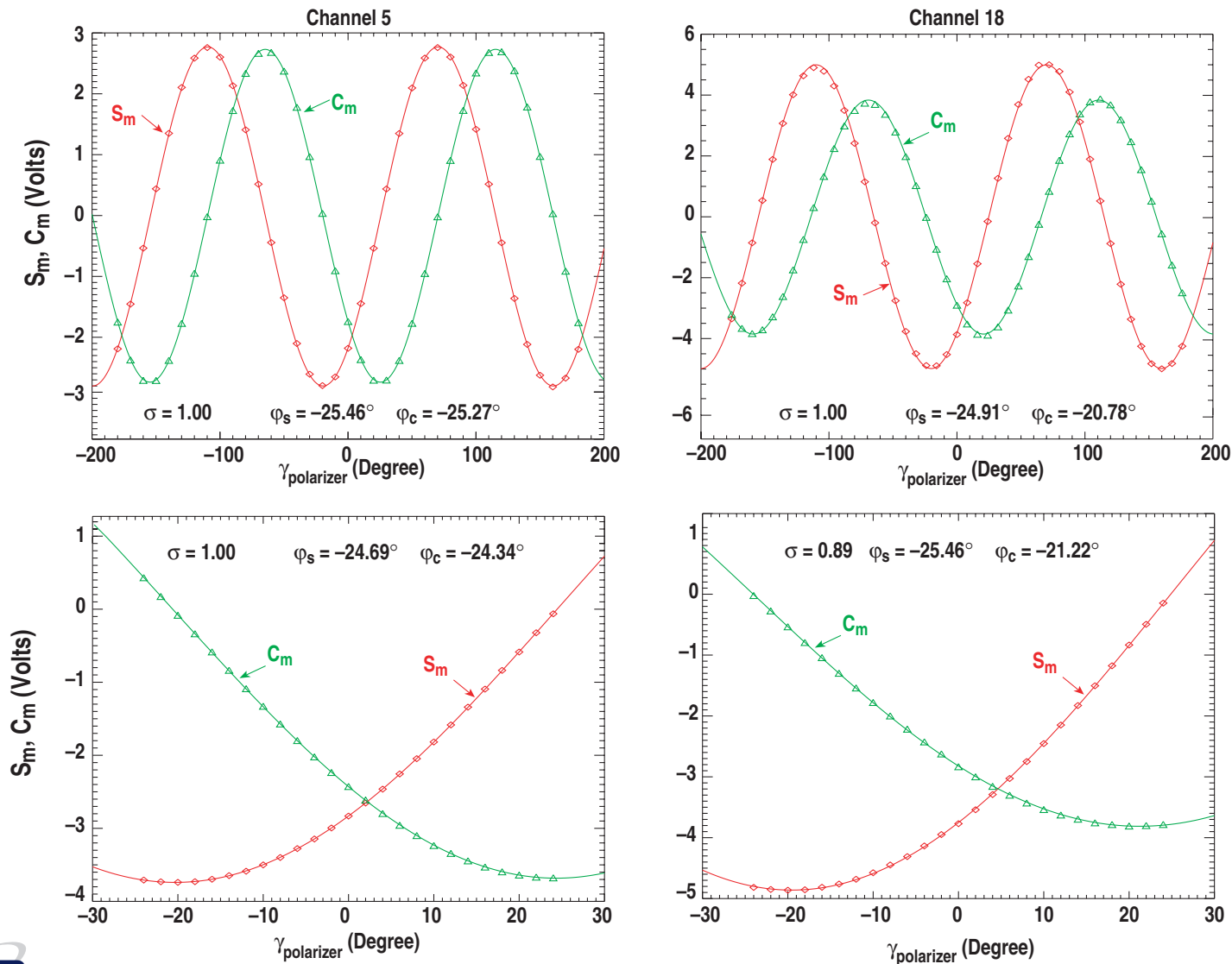
- In the tangent-slope model, σ was introduced only to improve the fit. There is no other rationale for it
- When scans spanning $\pm 180^\circ$ rather than $\pm 24^\circ$ are used to determine σ , its value is always found to be unity. (This can also be seen as a periodicity constraint)
- Modeling of the optical train also predicts $\sigma = 1$



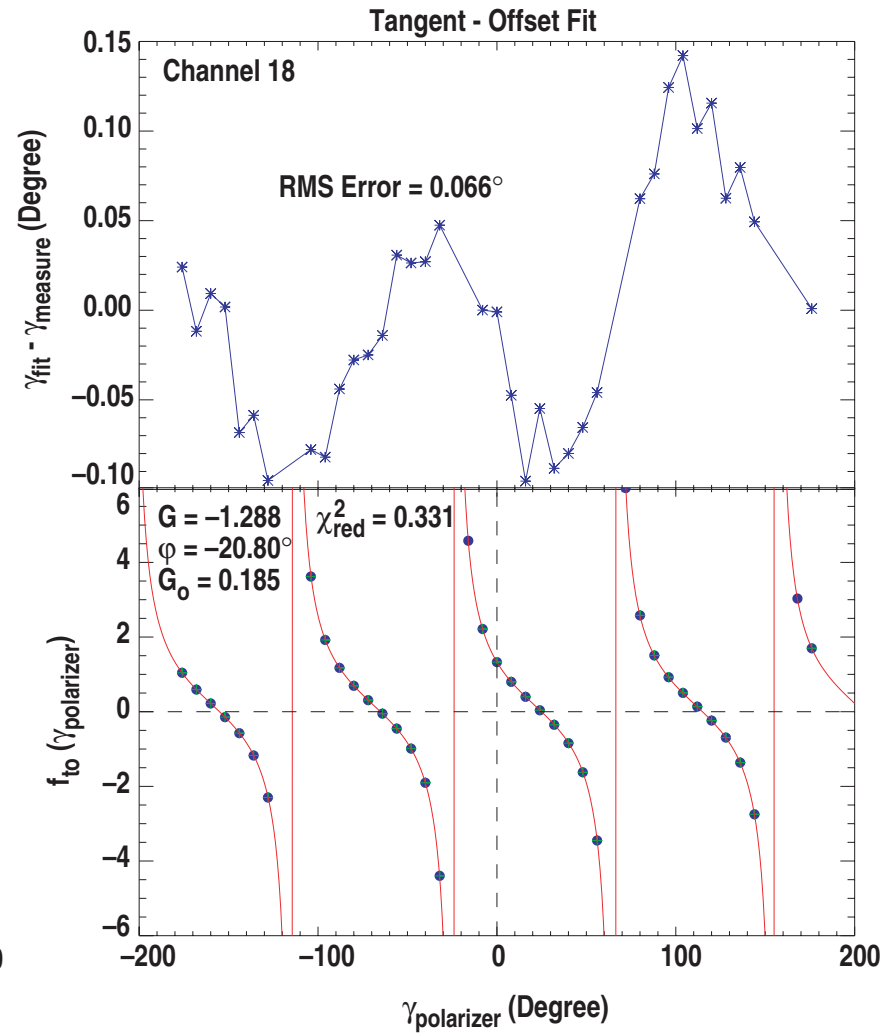
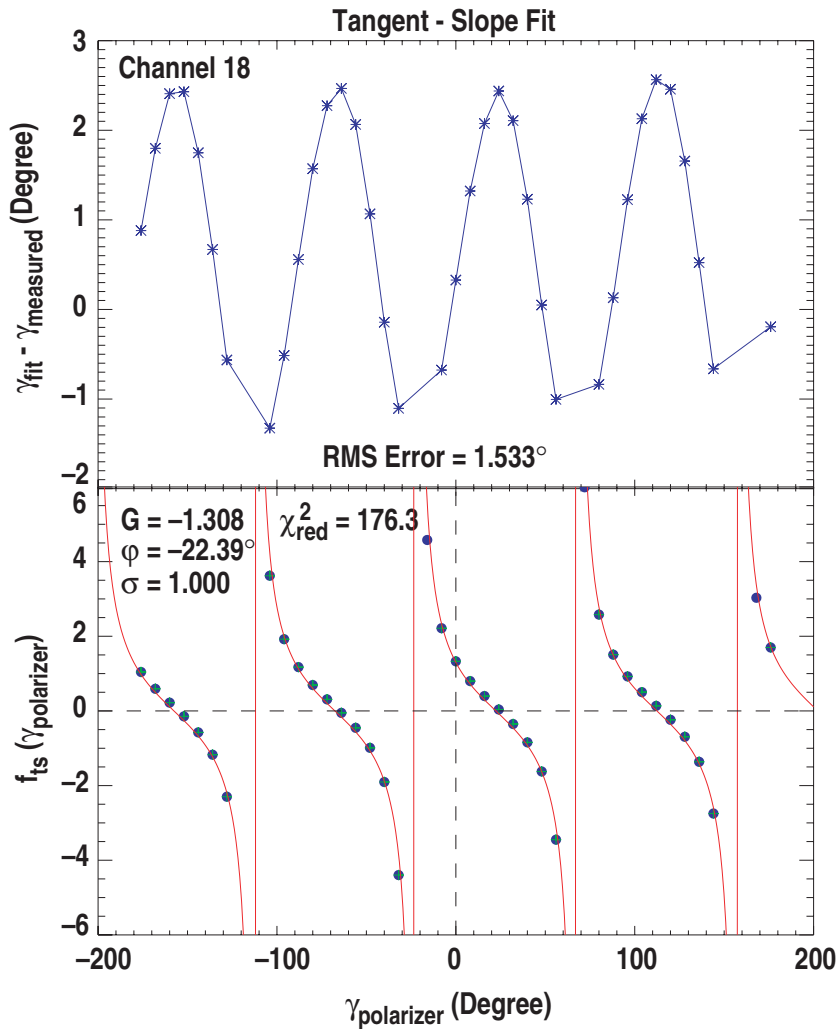
The Dielectric Mirror on the Edge Array
Appears to Induce a Phase Shift between
the S- and P-plane polarization components



The Value of σ Depends on the Scan Interval



Edge Array Poorly Fits Tangent-Slope Model



All Channels are Consistent with the Tangent-Offset Model

- Edge array fits tangent-offset model significantly better than the tangent-slope model
- For the tangential and radial arrays, the calibration data fits the tangent-slope model with $\sigma = 1$, as well as the tangent-offset model with $G_0 \approx 0$. The value of the phase is the same for both fits.



Phase Shift Exists between Sin/Cos Signals for Edge Array

- Fitting the raw data to

$$S_m = G_s \sin[2(\gamma + \varphi_s)] + G_{s0}$$

$$C_m = G_c \cos[2(\gamma + \varphi_c)] + G_{c0}$$

reveals $\varphi_s \neq \varphi_c$ for the edge array

- However, for the tangential and radial arrays, $\varphi_s \approx \varphi_c$
- Edge phase shift is suspected to be caused by the dielectric mirror in this optical train



Phase Shift is Fit Well by Tangent-Offset

- For $G_{s0} \approx G_{c0} \ll 1$

$$\frac{S_m}{C_m} = \frac{G_s \sin[2(\gamma + \varphi_s)]}{G_c \cos[2(\gamma + \varphi_c)]}$$

$$= \frac{G_s}{G_c} \tan[2(\gamma + \varphi_c)] \cos[2(\varphi_s - \varphi_s)] + \frac{G_s}{G_c} \sin[2(\varphi_s - \varphi_s)]$$

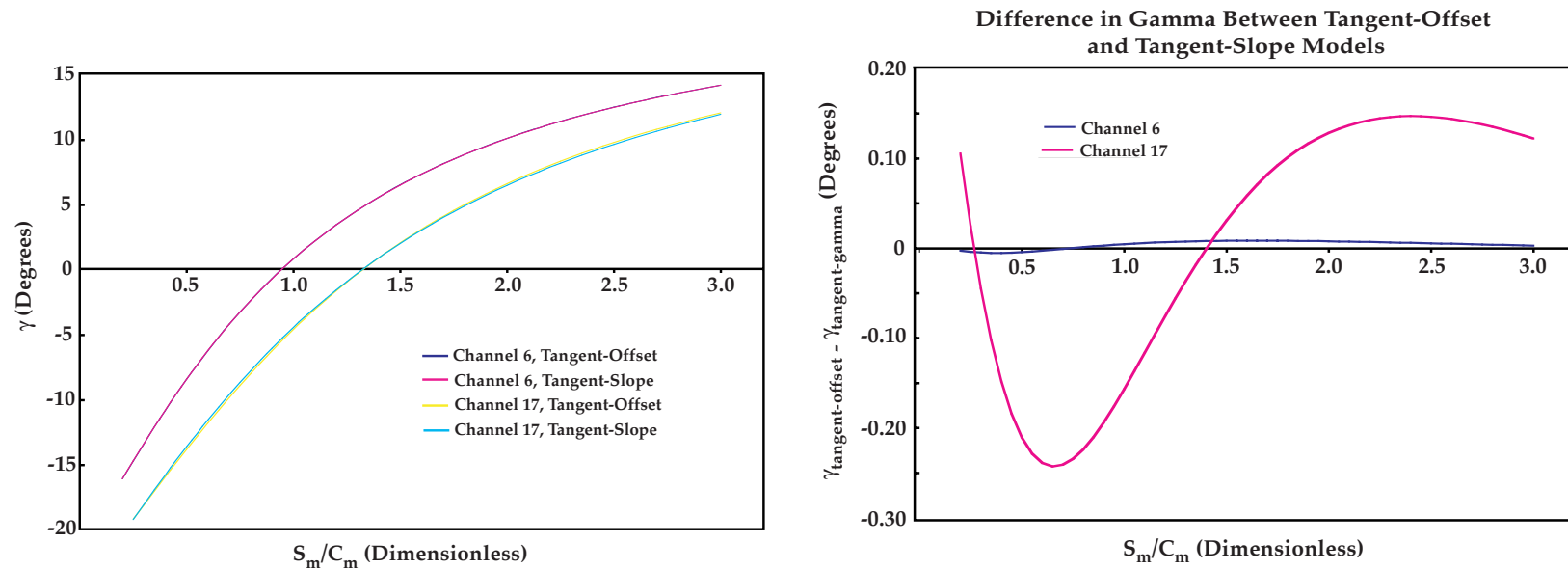
- This is the tangent-offset form with

$$G = \frac{G_s}{G_c} \cos[2(\varphi_s - \varphi_c)], \quad G_0 = G \tan[2(\varphi_s - \varphi_c)]$$

- This reduces to the tangent-slope form when $\varphi_s = \varphi_c$ and $\sigma = 1$



Correction only Significant on Edge Array



- Tangent-offset and tangent-slope forms agree for tangential and radial arrays
- Forms differ for edge array by $\pm 0.25^\circ$

Quality of Fit Improves with Number of Samples

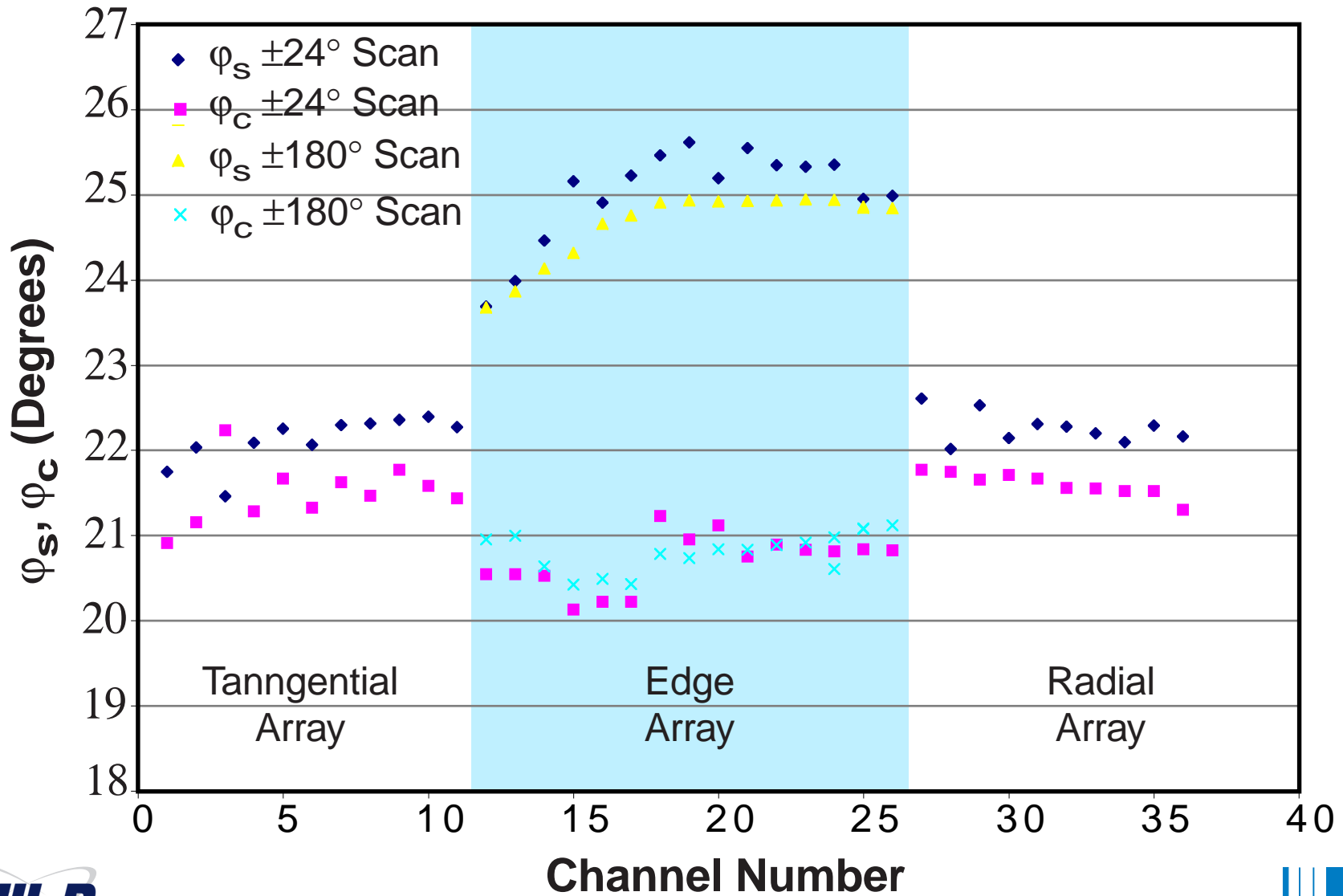
- Coefficients not completely independent leading to apparently large errors

Scan	Range	Step	G	$\epsilon(G)$	ϕ	$\epsilon(\phi)$	G_0	$\epsilon(G_0)$	$(\chi_{\text{red}})^2$
1	48°	2°	-1.318	± 1.111	-21.03°	$\pm 10.67^\circ$	0.173	± 0.469	0.019
2	360°	8°	-1.316	± 0.239	-21.06°	$\pm 2.25^\circ$	0.175	± 0.259	0.164
3	360°	2°	-1.317	± 0.129	-21.09°	$\pm 1.34^\circ$	0.174	± 0.149	0.126

- Error is reduced as the range and number of sample points is increased
- Fit coefficients do not change as error is reduced



φ_s and φ_c Differ only on the Edge Array

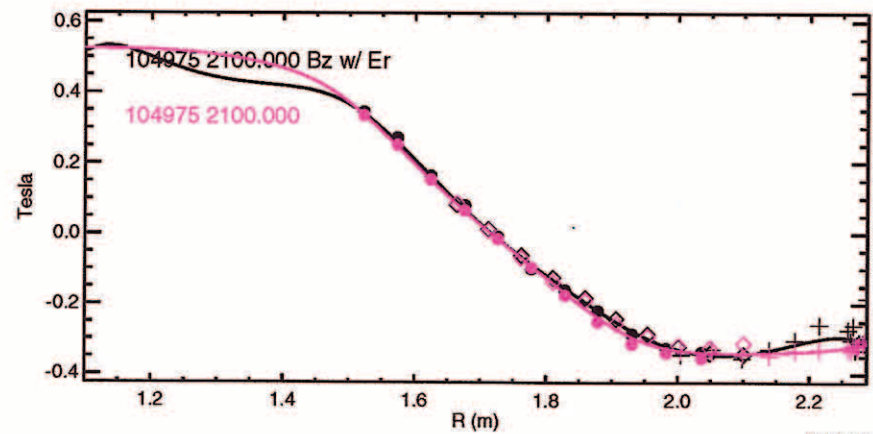
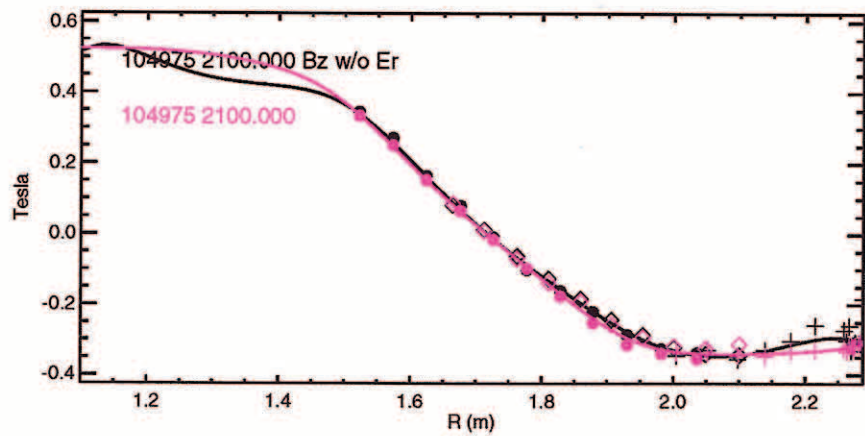
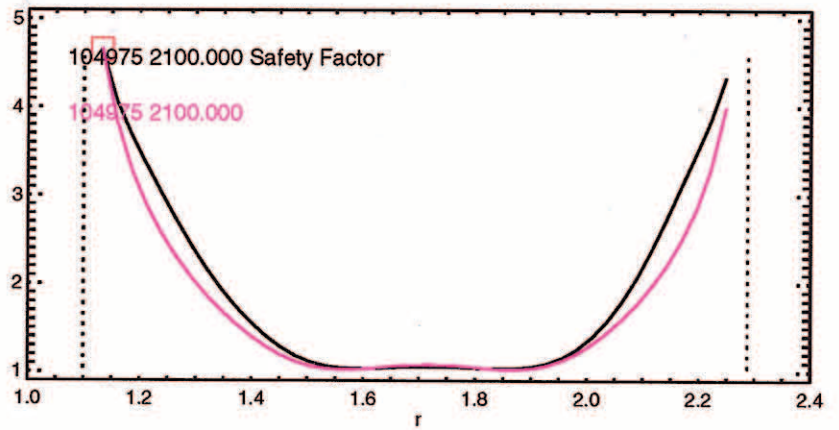
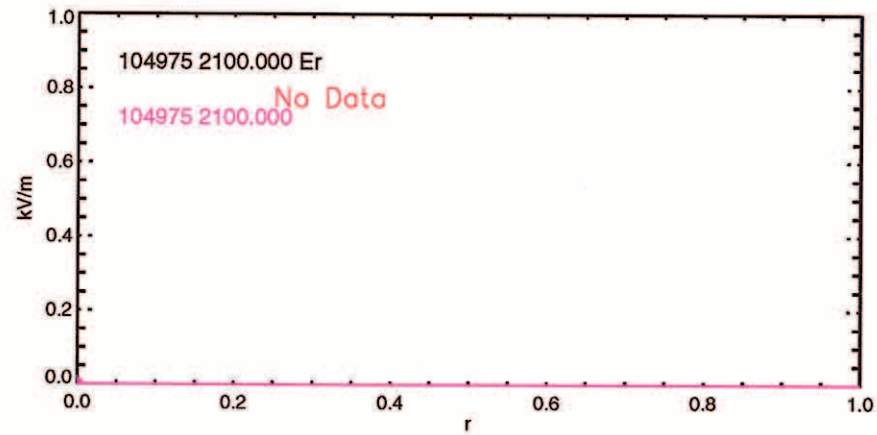
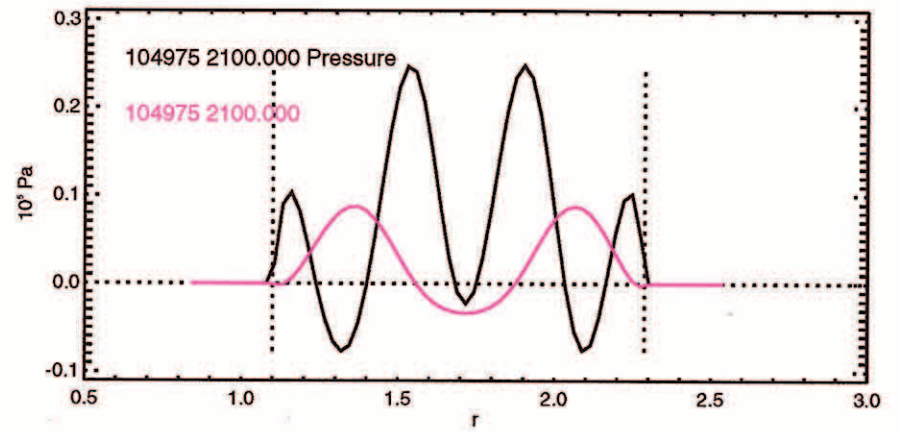
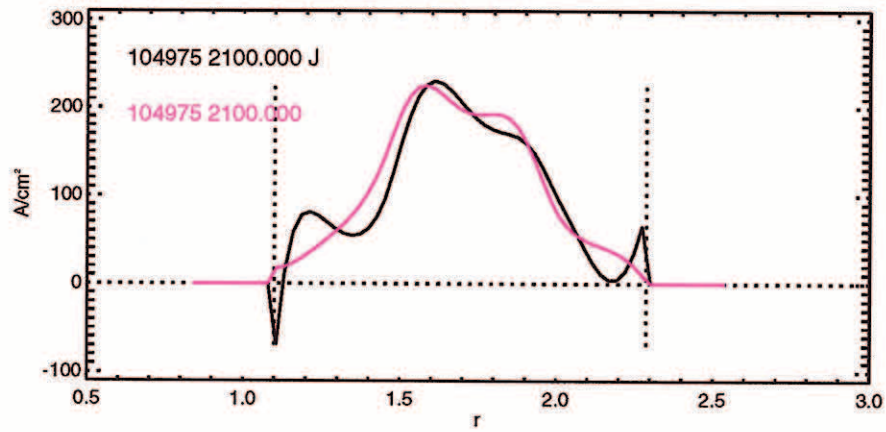


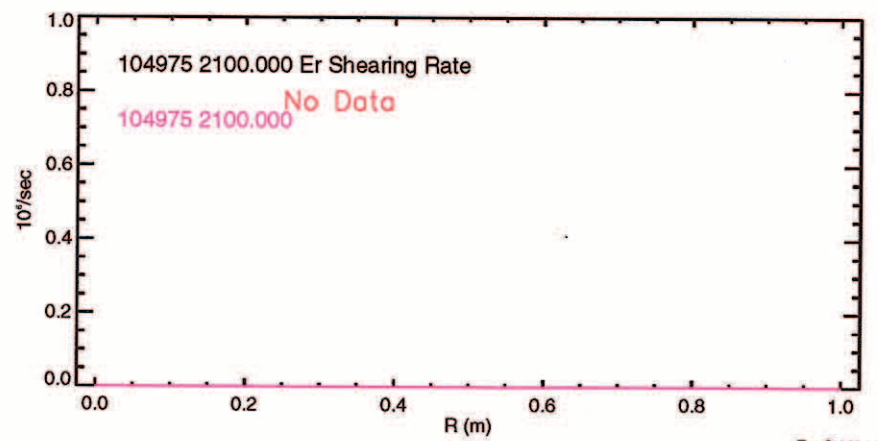
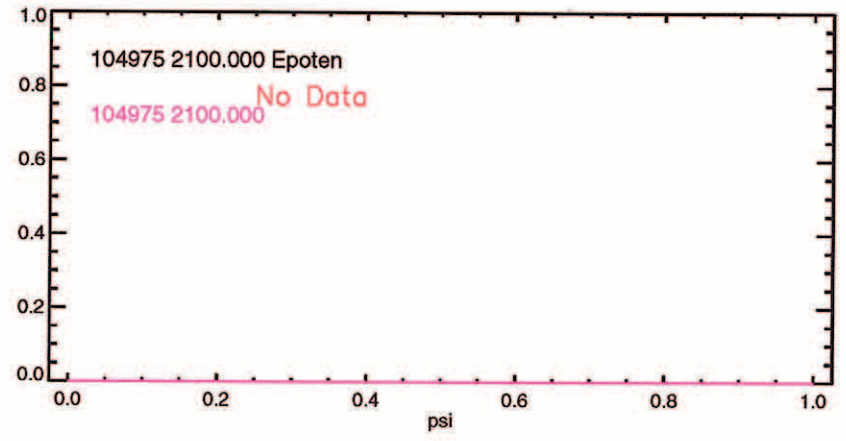
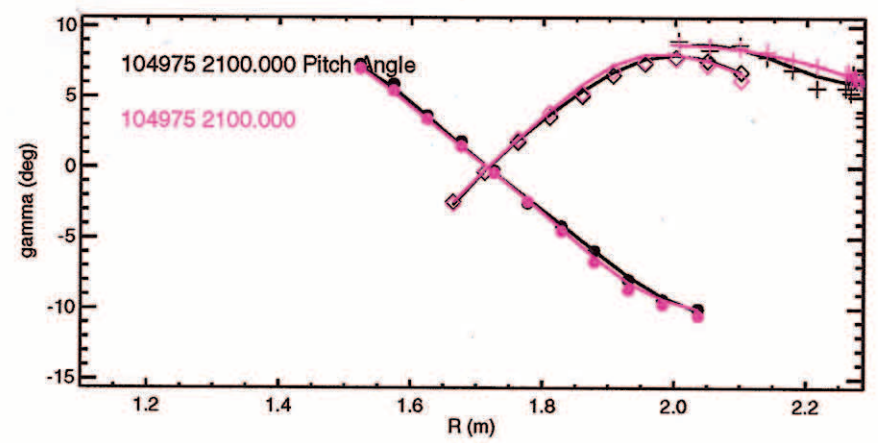
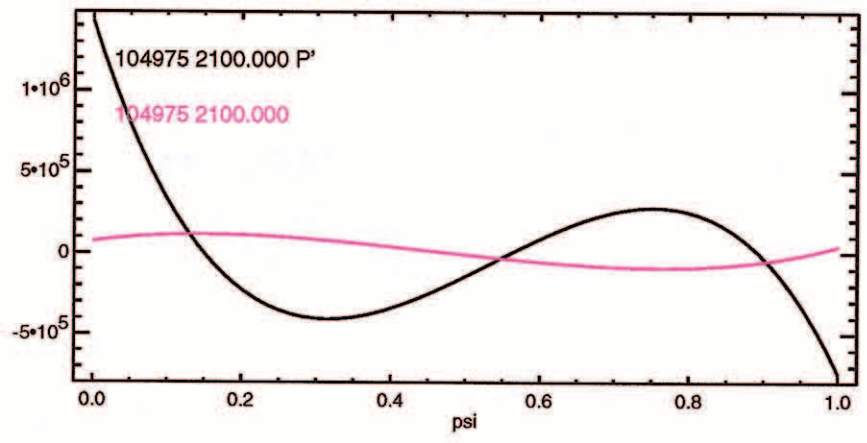
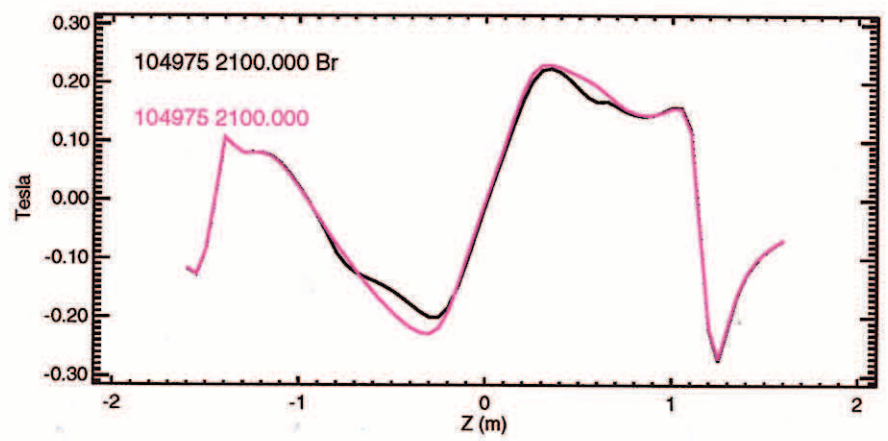
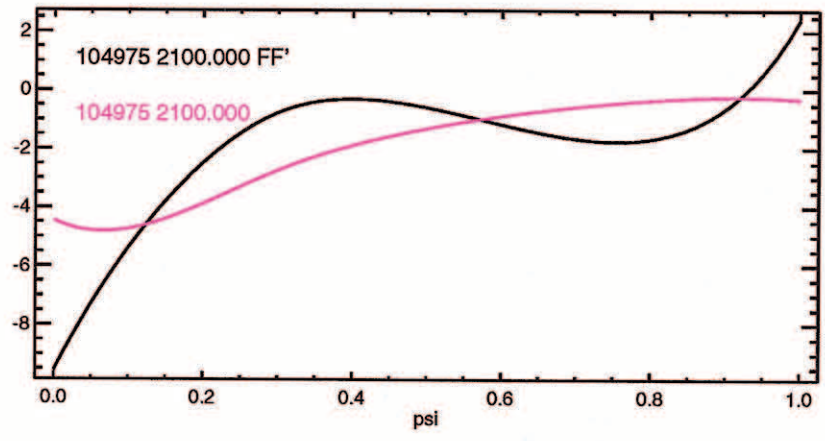
Comparison of EFITs using Pitch Angles
Computed with the Tangent-Slope Model
(Curves in Black) and the Tangent-Offset
Model (Curves in Magenta)

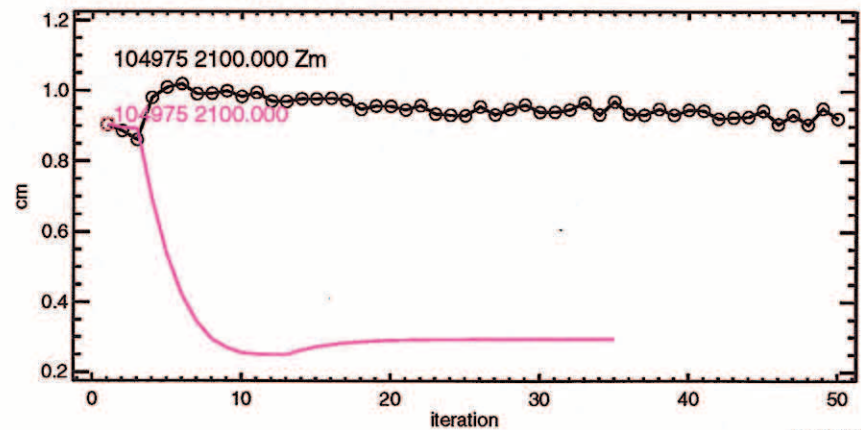
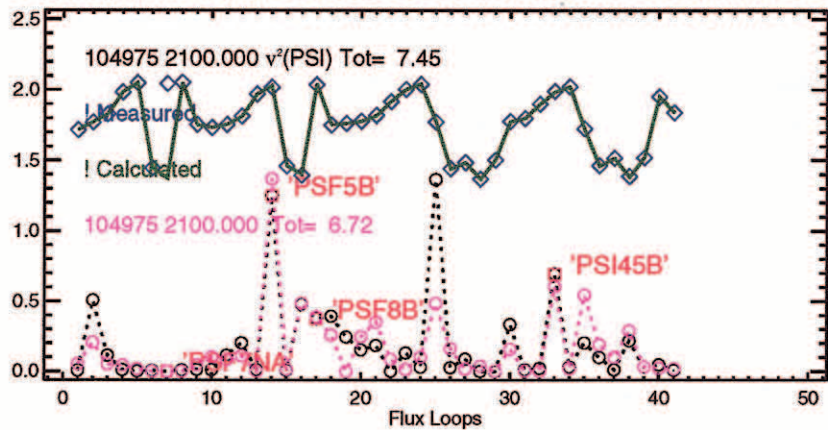
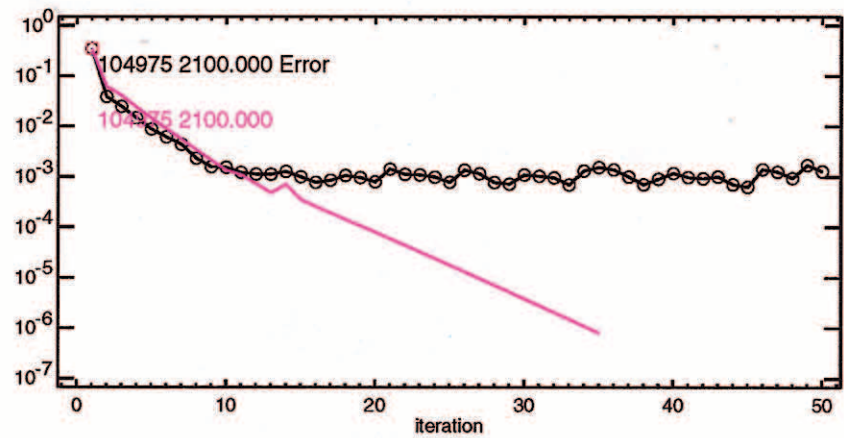
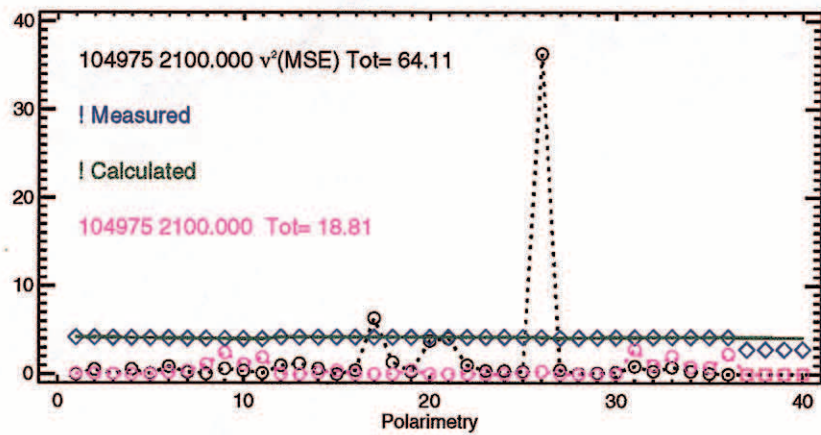
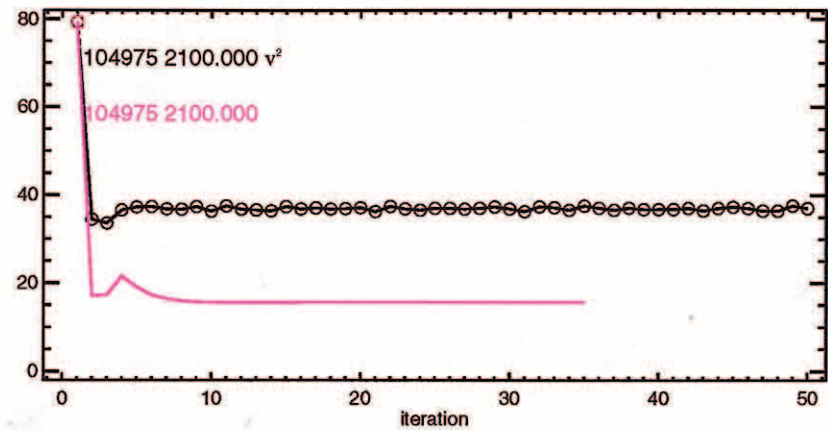
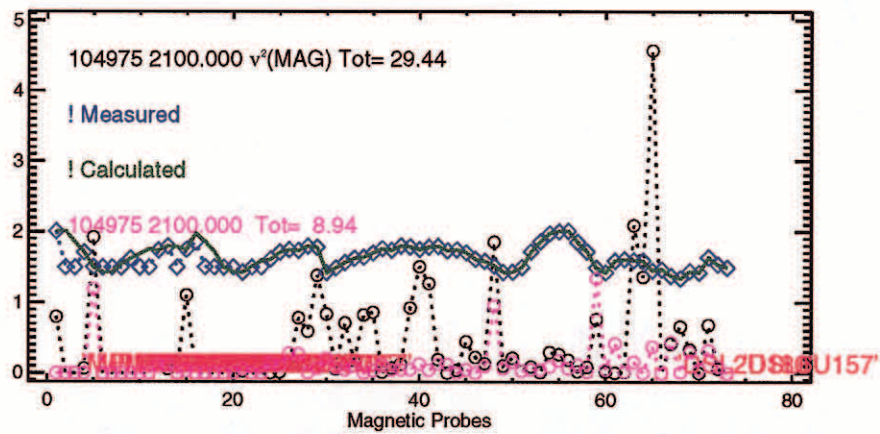


Ohmic, L-mode, Ip-ramp, No E_r

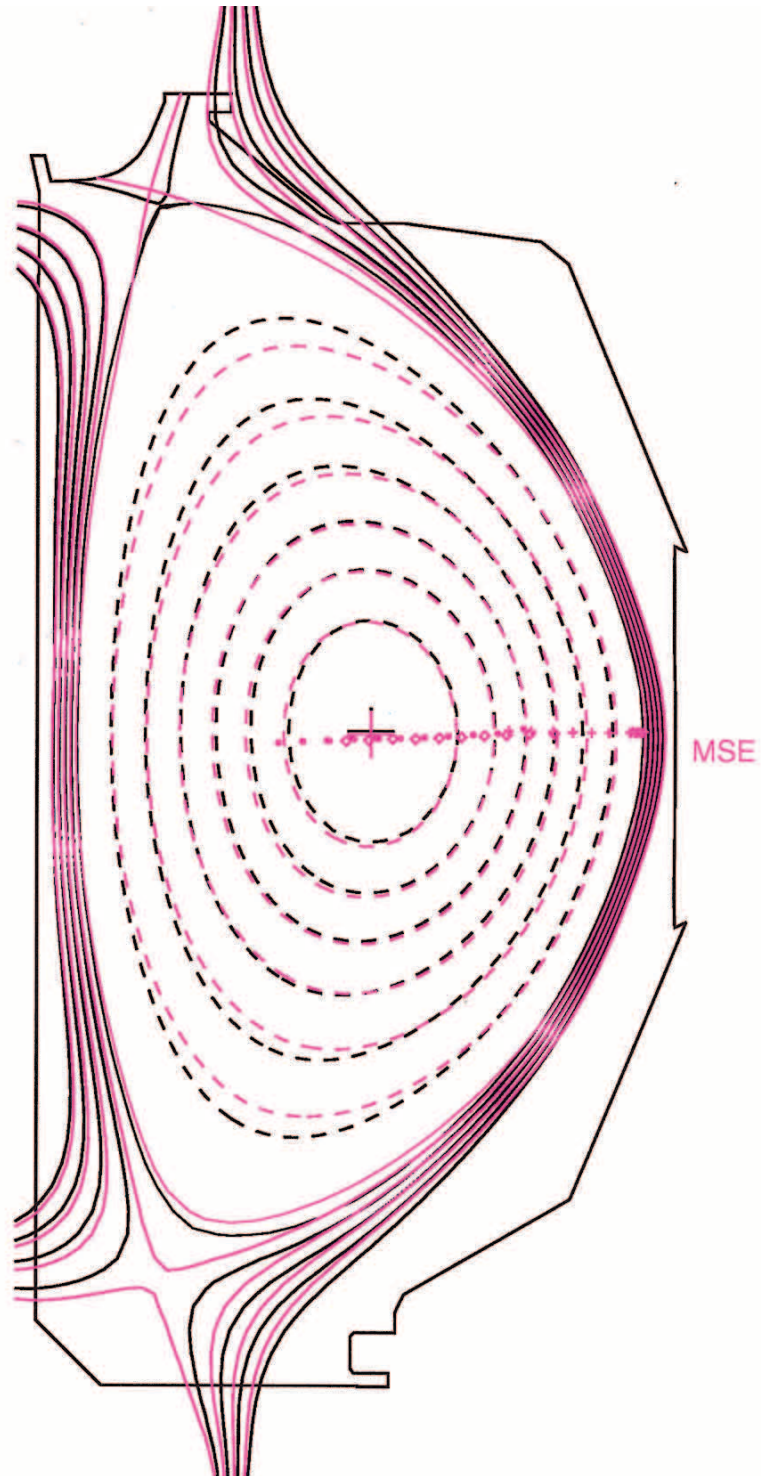






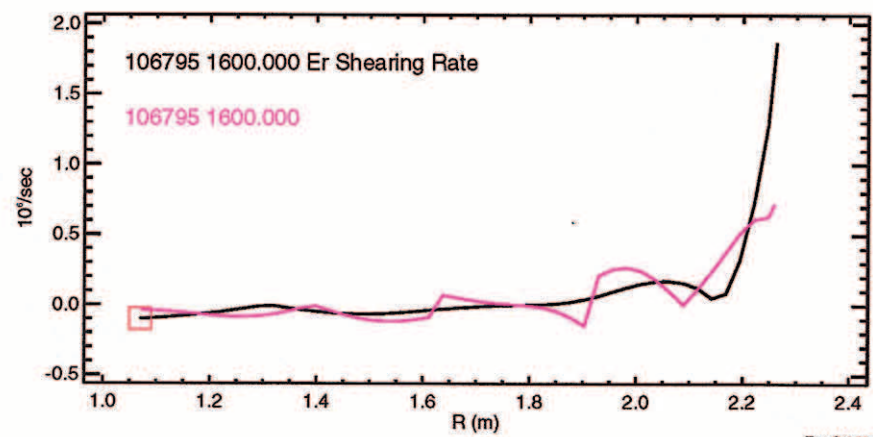
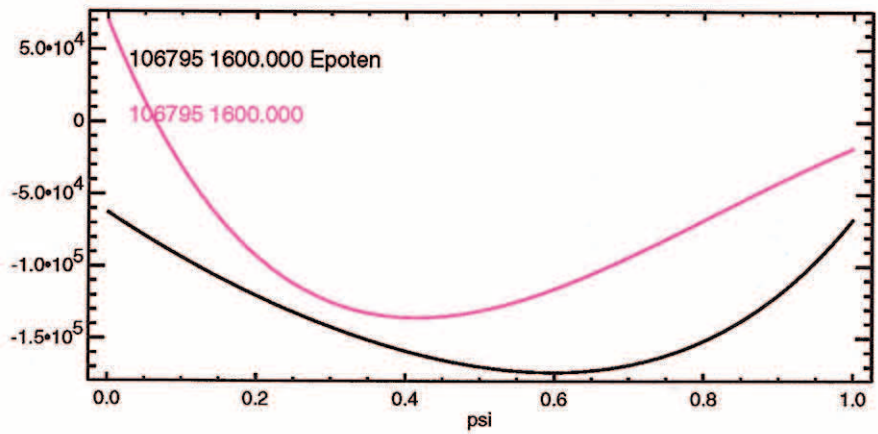
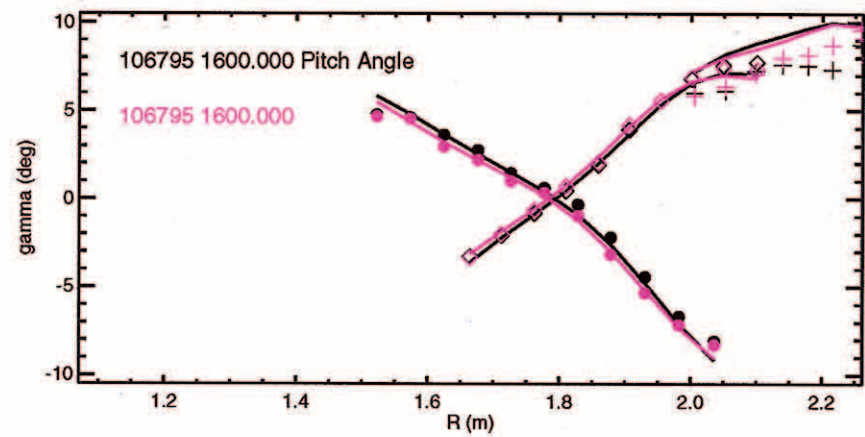
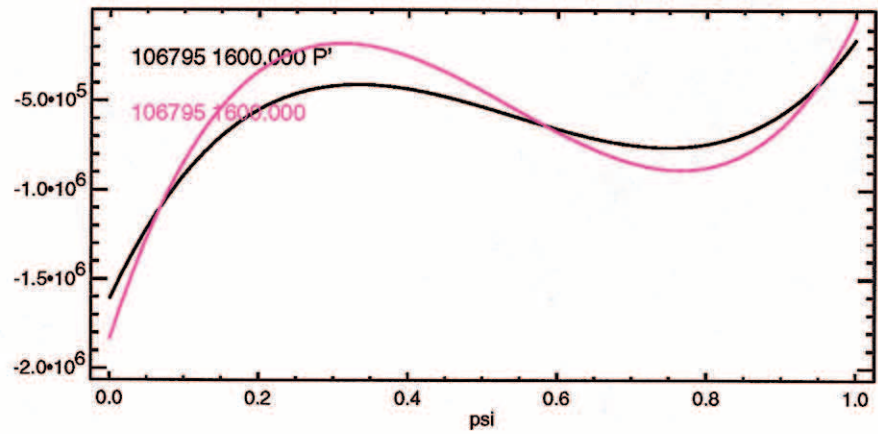
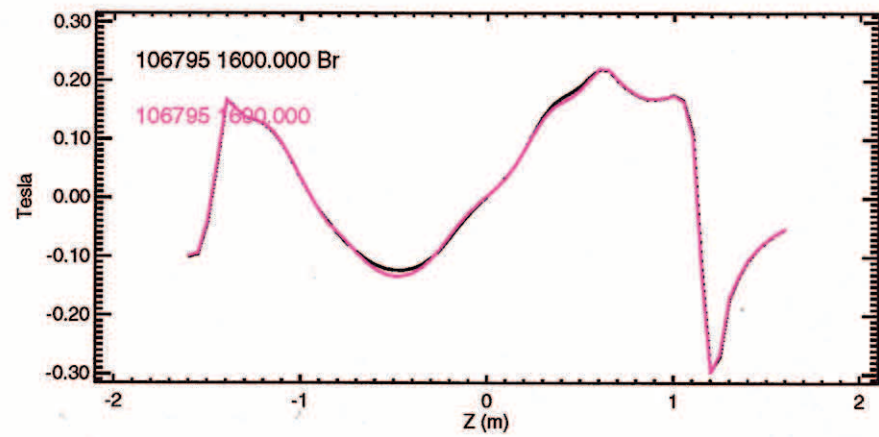
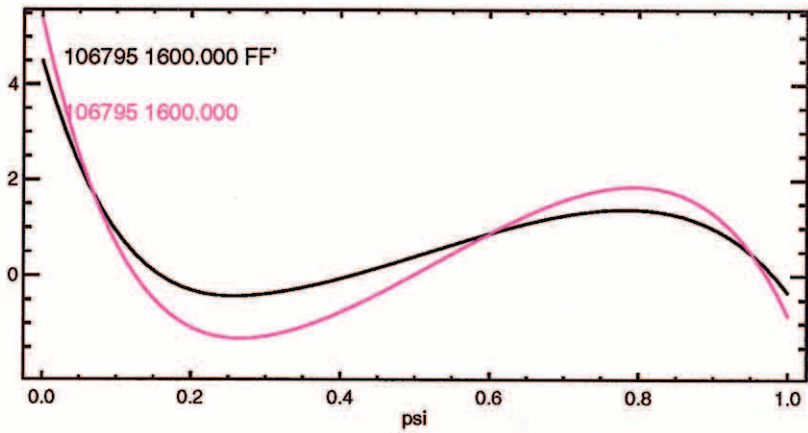


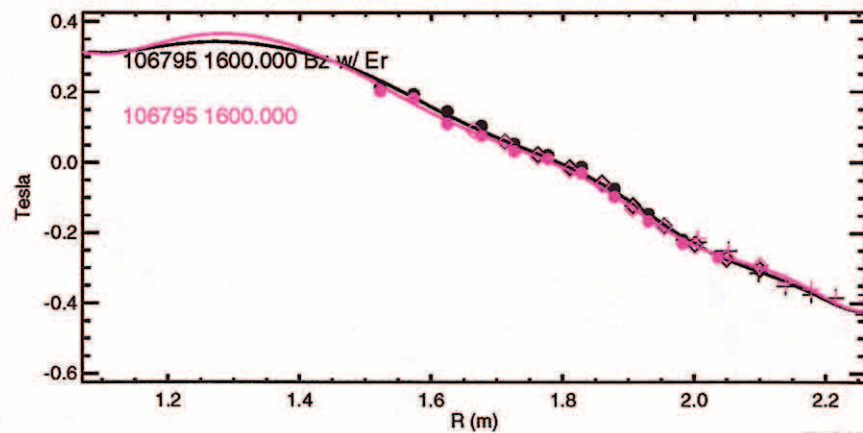
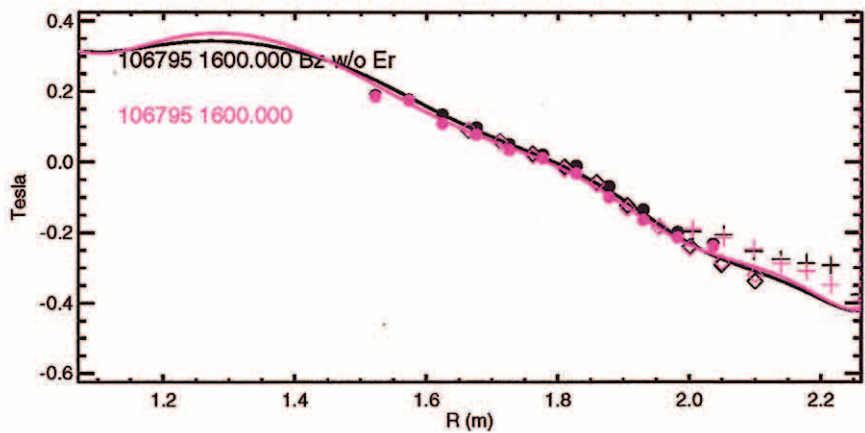
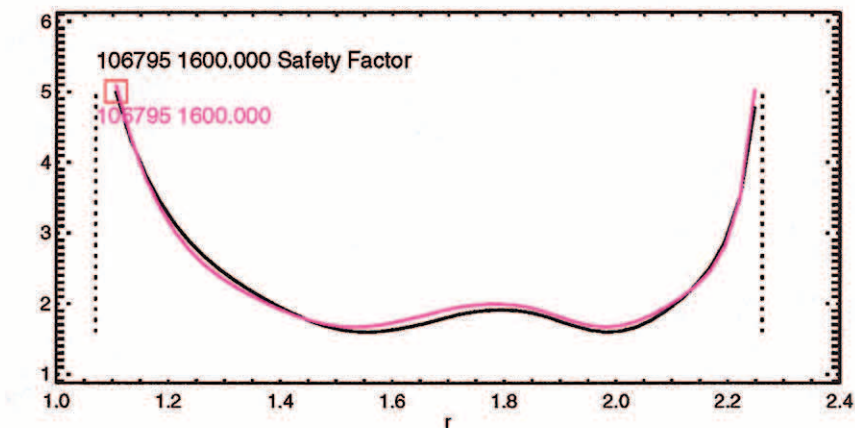
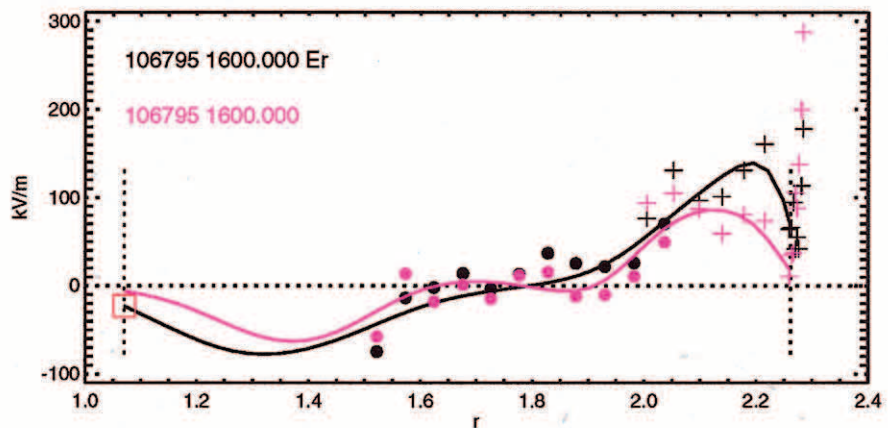
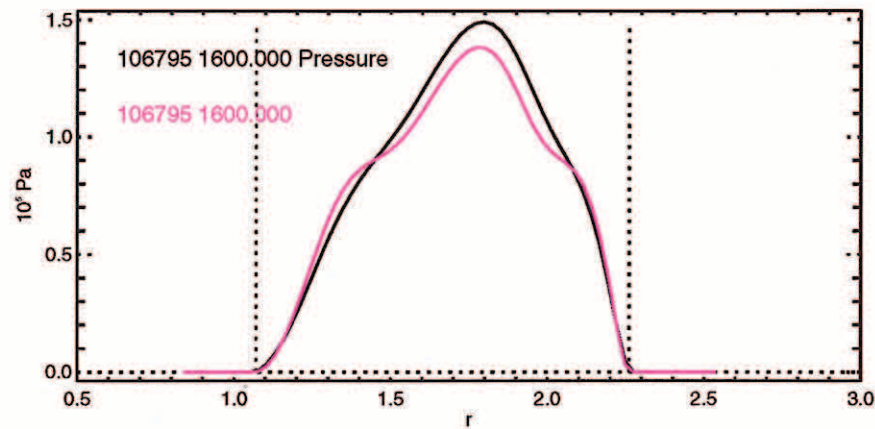
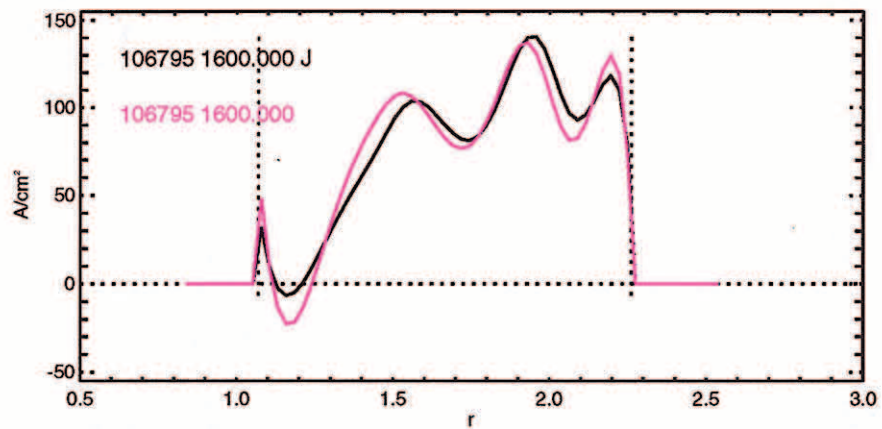
chi**2	15.664
Rout(m)	1.695
Zout(m)	0.061
a(m)	0.597
elong	1.816
utri	0.744
ltri	0.453
indent	0.000
V (m**3)	19.254
A (m**2)	1.881
W (MJ)	0.103
betaT(%)	0.203
betaP	0.124
betaN	0.221
ln	0.918
Li	1.243
error(e-4)	0.008
q1	9.769
q95	4.997
dsep(m)	0.062
Rm(m)	1.716
Zm(m)	0.003
Rc(m)	1.673
Zc(m)	0.010
betaPd	0.201
betaTd	0.328
Wdia(MJ)	0.167
Ipmeas(MA)	1.157
BT(O)(T)	-2.105
Ipfit(MA)	1.155
Rmidin(m)	1.098
Rmidout(m)	2.290
gapin(m)	0.082
gapout(m)	0.062
gaptop(m)	0.070
gapbot(m)	0.277
Zts(m)	0.749
Rvsin(m)	1.138
Zvsin(m)	1.170
Rvsout(m)	1.314
Zvsout(m)	1.348
Rsep1(m)	1.266
Zsep1(m)	-1.141
Rsep2(m)	1.250
Zsep2(m)	1.146
psib(Vs/R)	-0.013
elongm	1.313
qm	1.079
nev1(e19)	59.588
nev2(e19)	2.163
nev3(e19)	2.065
ner0(e19)	1.861
n/nc	-0.705
dRsep	0.010
qmin	1.025
rhoqmin	0.223

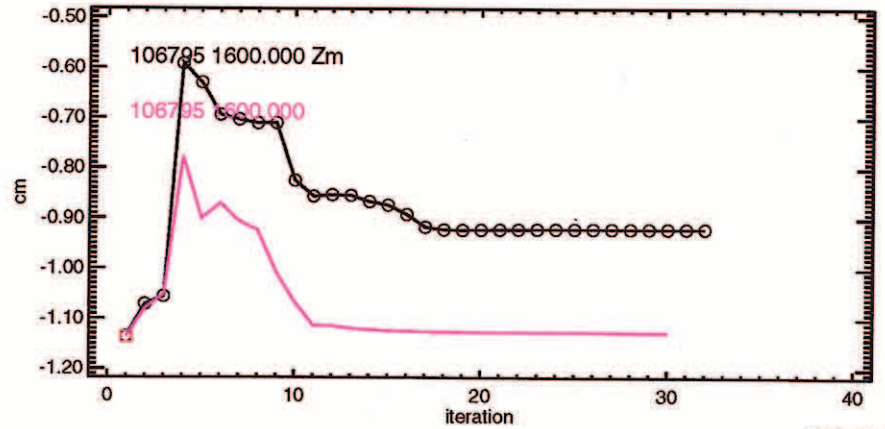
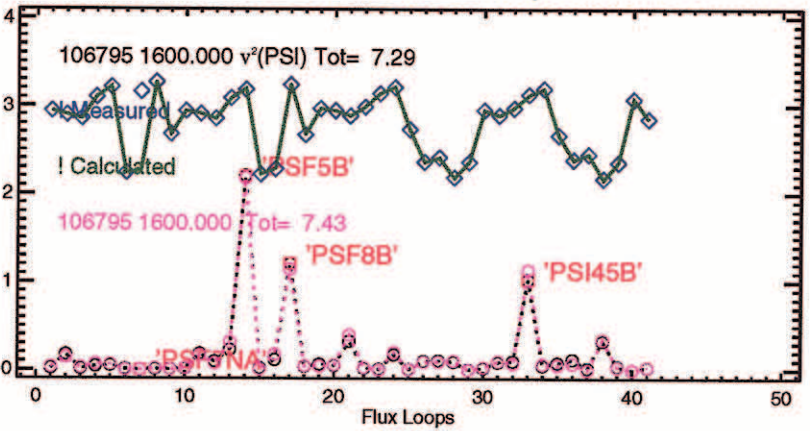
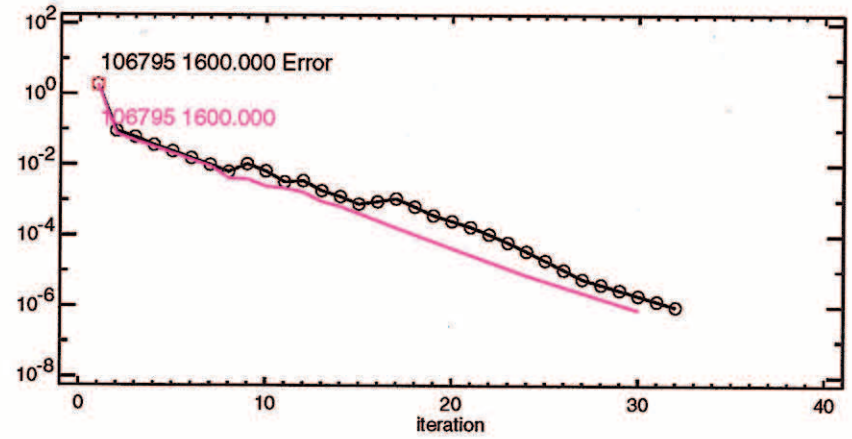
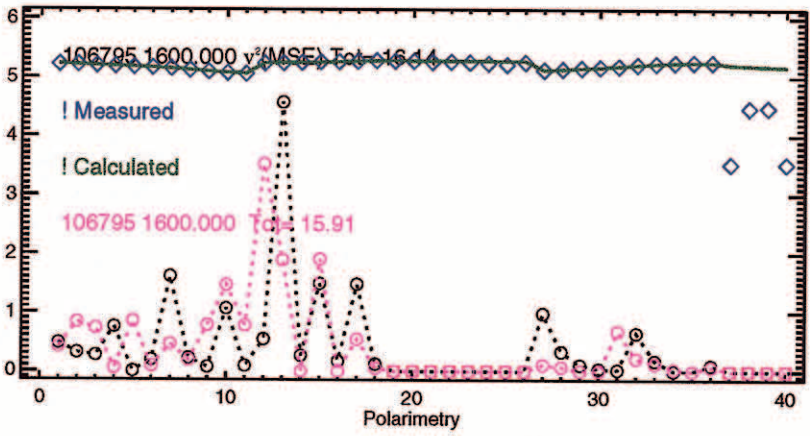
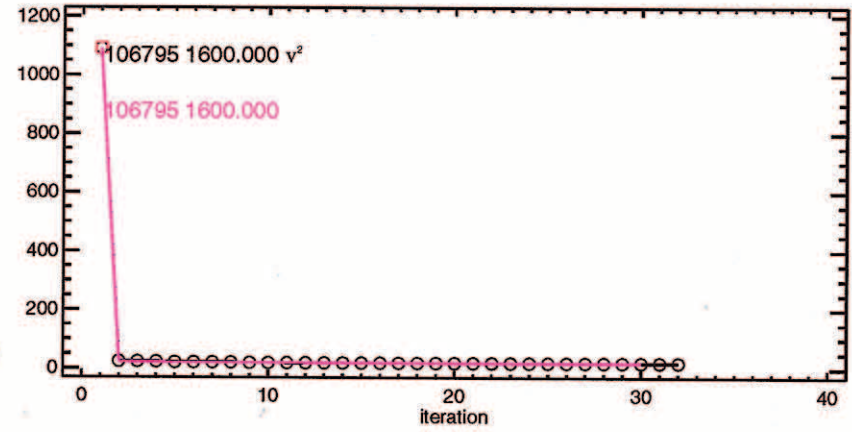
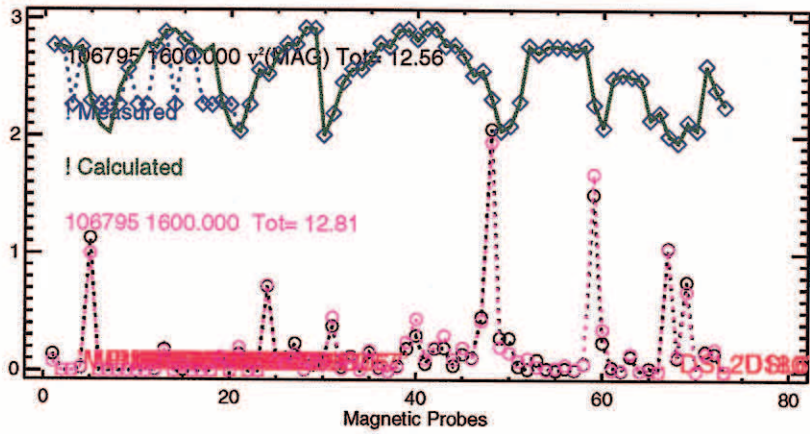


Typical Thrust 2 Shot with E_r

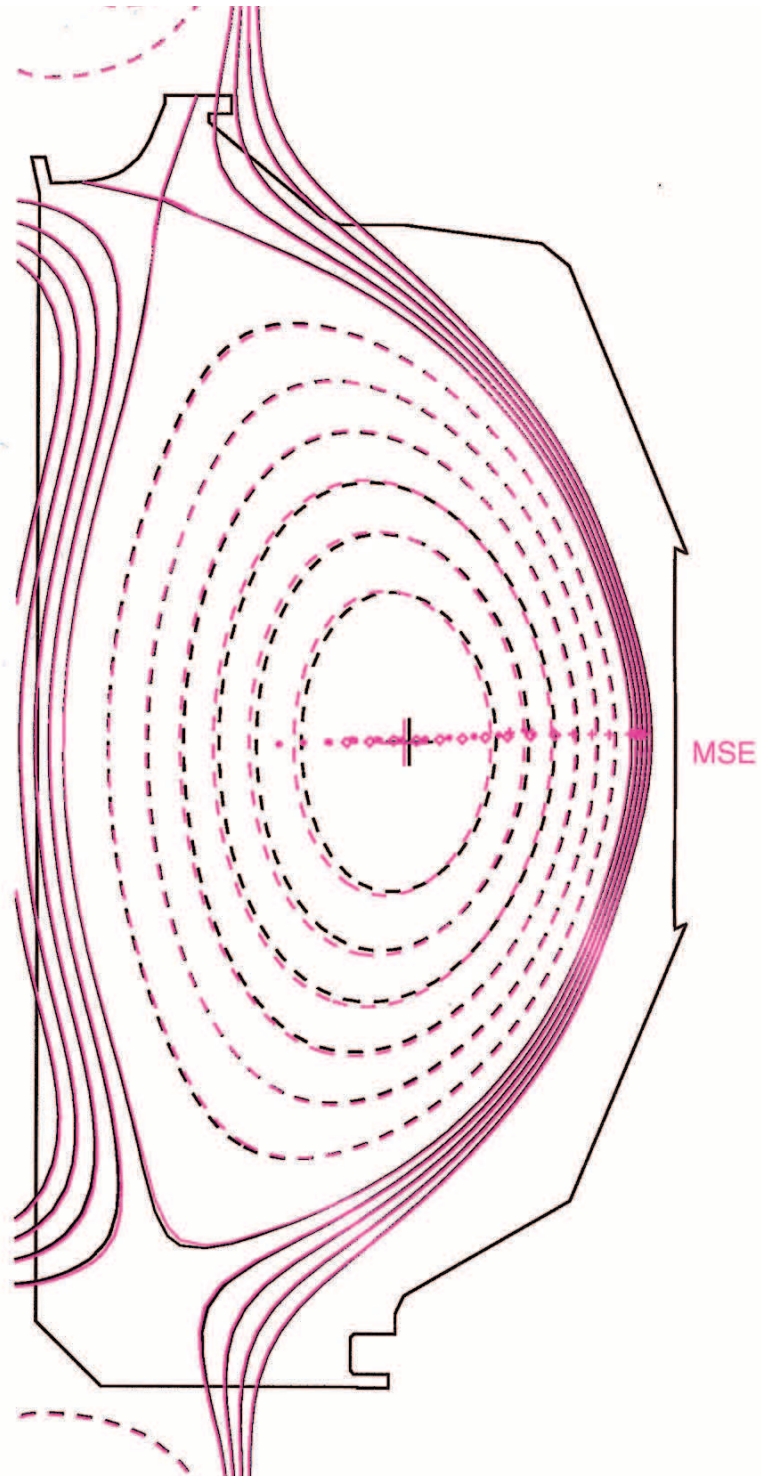






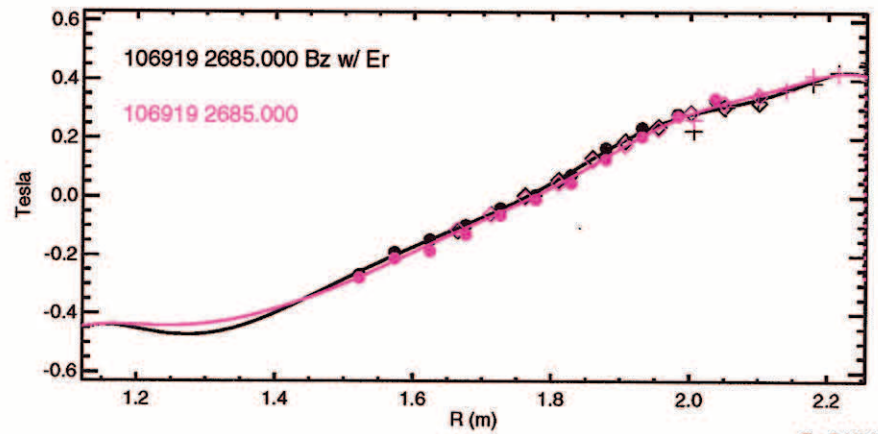
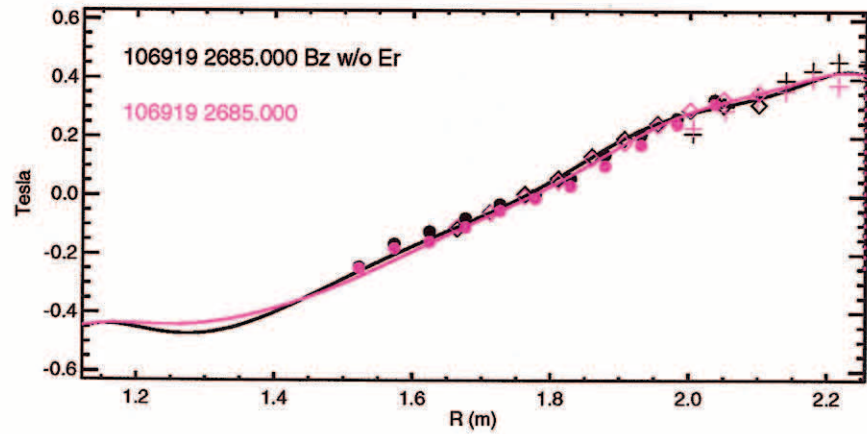
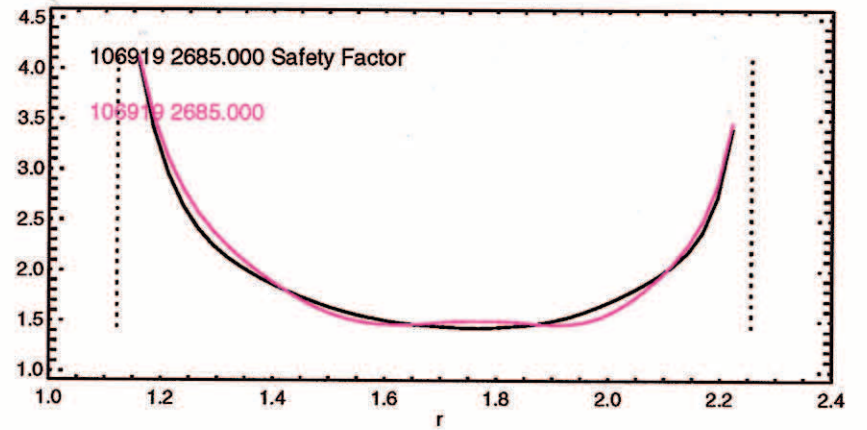
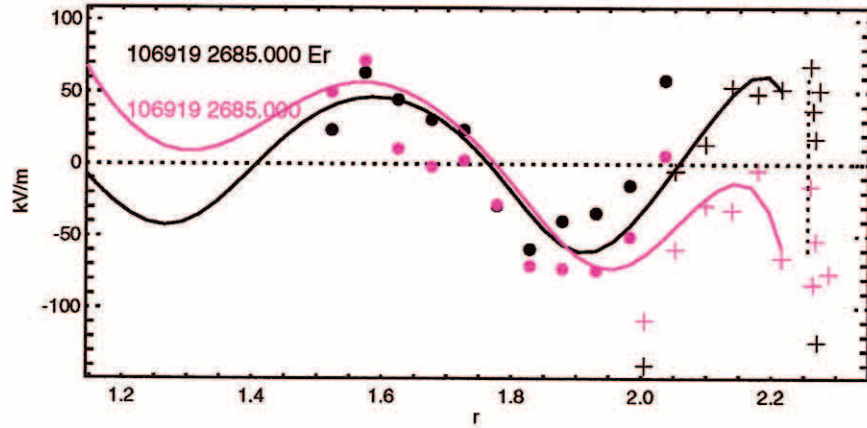
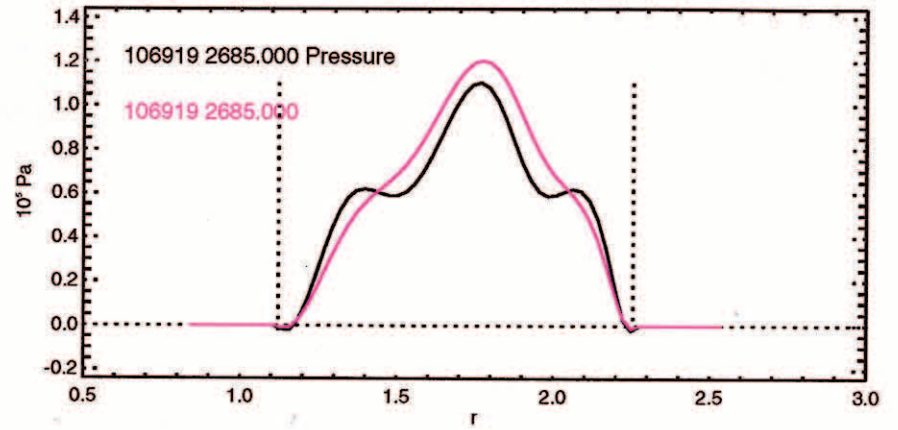
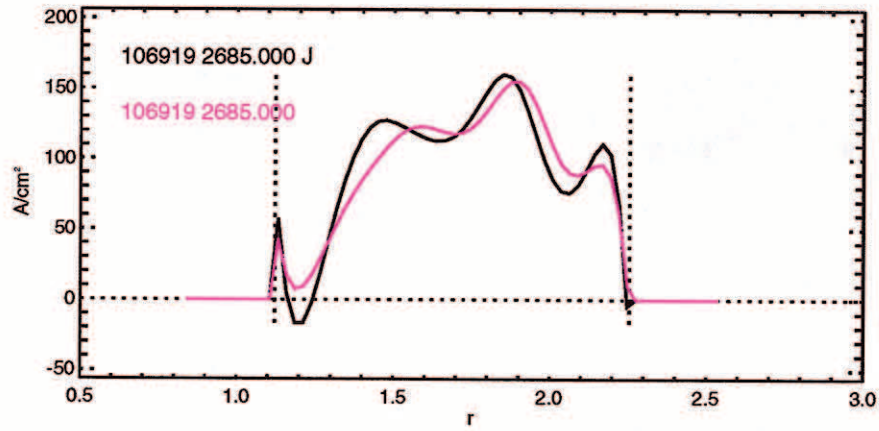


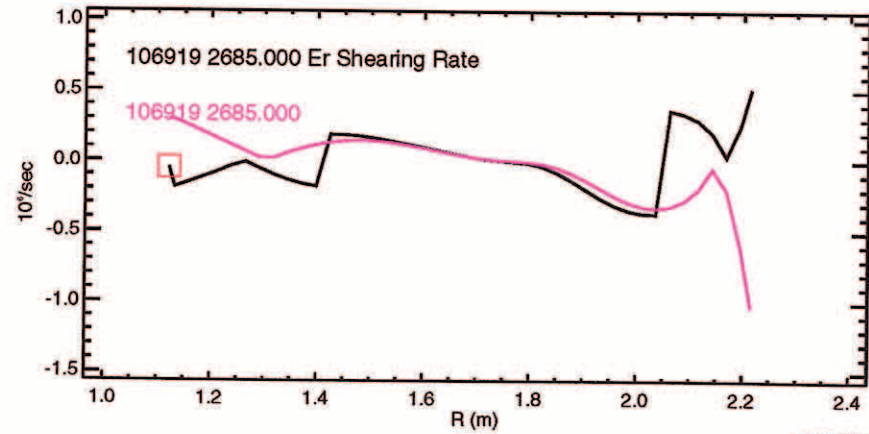
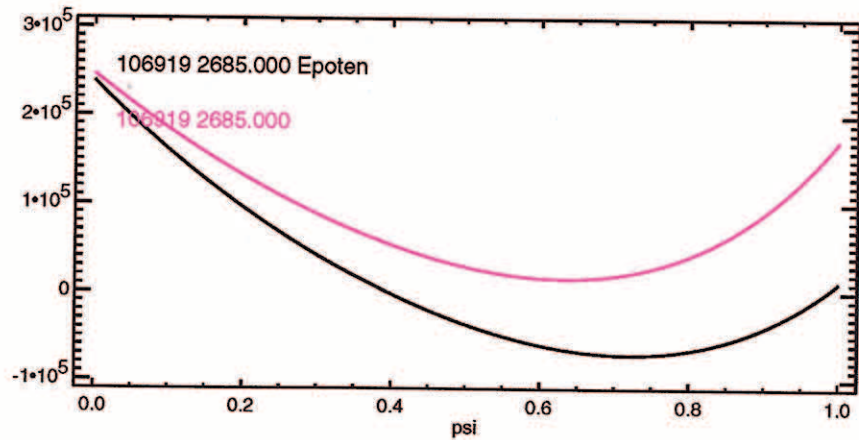
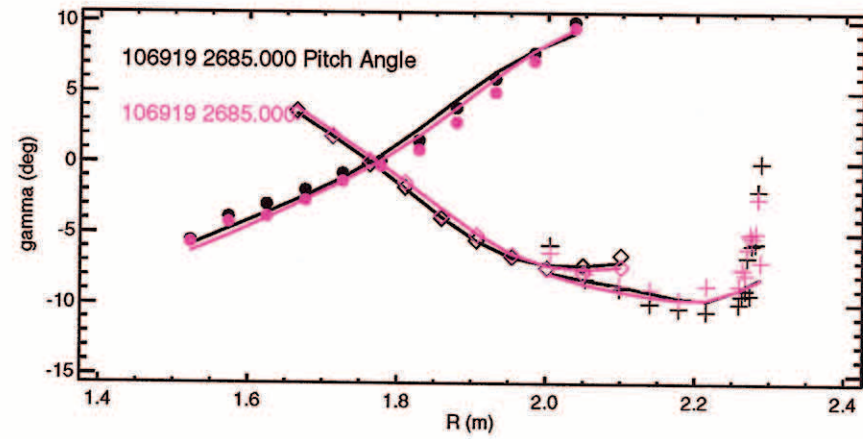
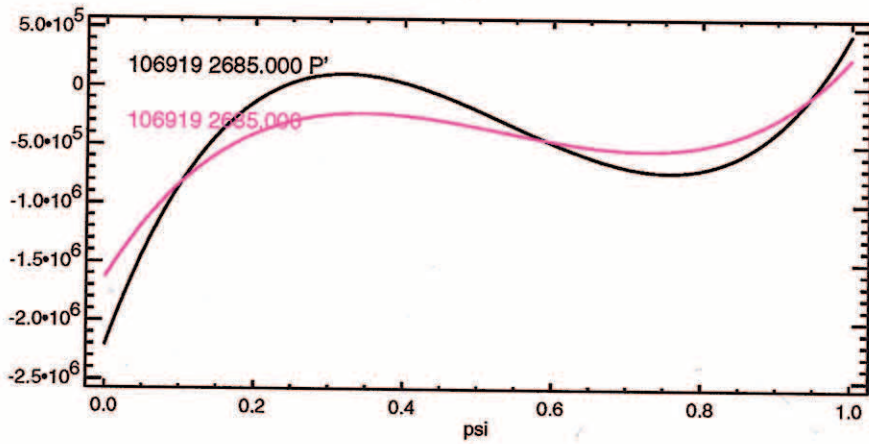
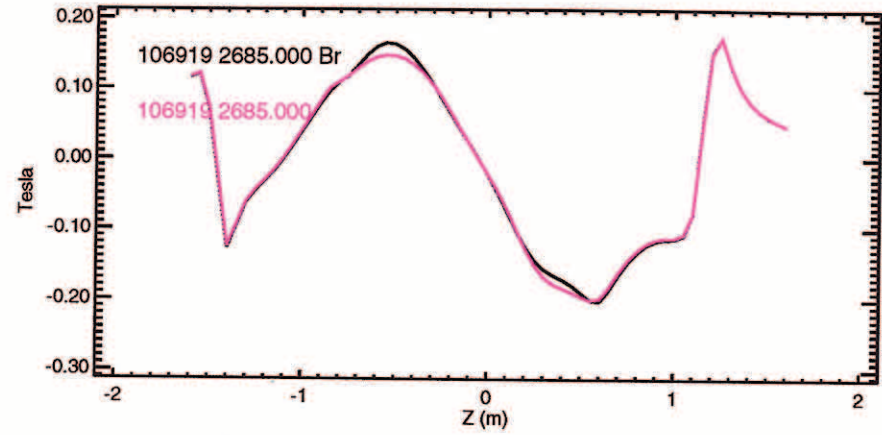
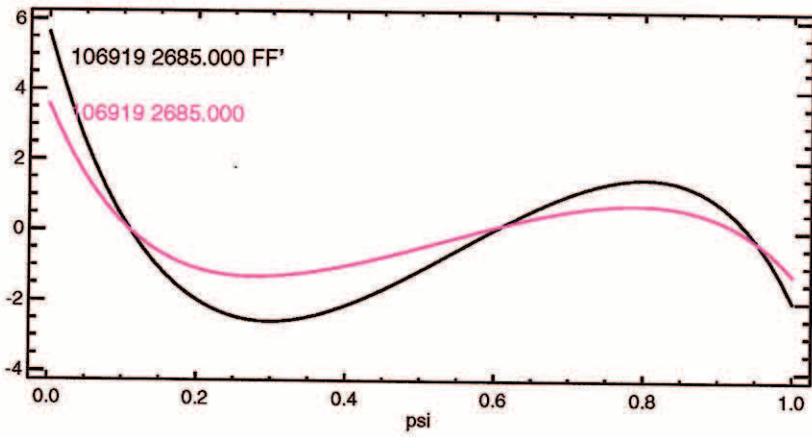
chi**2	20.243
Rout(m)	1.666
Zout(m)	0.031
a(m)	0.595
elong	1.849
utri	0.661
ltri	0.495
indent	0.000
V (m**3)	18.958
A (m**2)	1.863
W (MJ)	1.679
betaT(%)	4.199
betaP	1.873
betaN	3.872
ln	1.084
Li	0.805
error(e-4)	0.008
q1	7.387
q95	5.115
dsep(m)	0.055
Rm(m)	1.784
Zm(m)	-0.011
Rc(m)	1.771
Zc(m)	-0.008
betaPd	1.925
betaTd	4.315
Wdia(MJ)	1.726
lpmeas(MA)	1.212
BT(O)(T)	-1.847
lpfit(MA)	1.213
Rmidin(m)	1.071
Rmidout(m)	2.259
gapin(m)	0.055
gapout(m)	0.093
gaptop(m)	0.095
gapbot(m)	0.261
Zts(m)	0.743
Rvsin(m)	1.108
Zvsin(m)	1.166
Rvsout(m)	1.345
Zvsout(m)	1.348
Rsep1(m)	1.272
Zsep1(m)	-1.136
Rsep2(m)	1.272
Zsep2(m)	1.131
psib(Vs/R)	0.244
elongm	1.641
qm	1.995
nev1(e19)	10.604
nev2(e19)	6.289
nev3(e19)	5.962
ner0(e19)	5.789
n/nc	-0.502
dRsep	0.004
qmin	1.668
rhoqmin	0.378

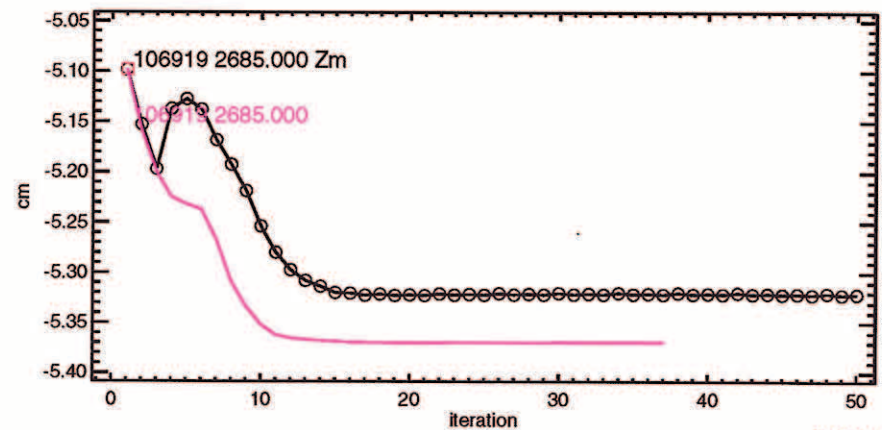
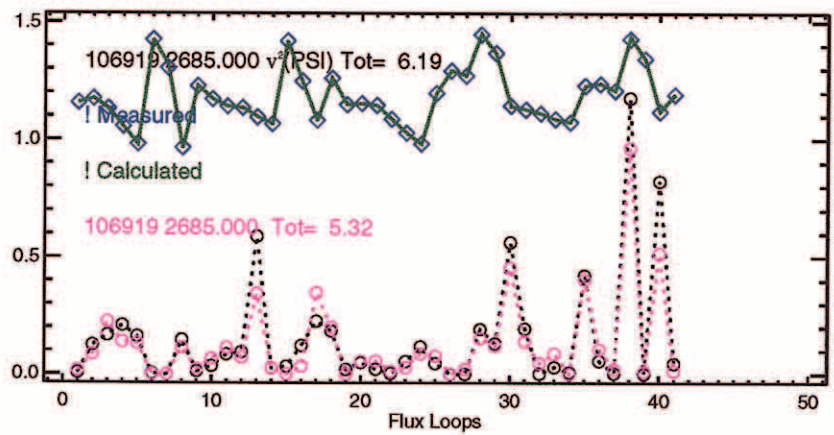
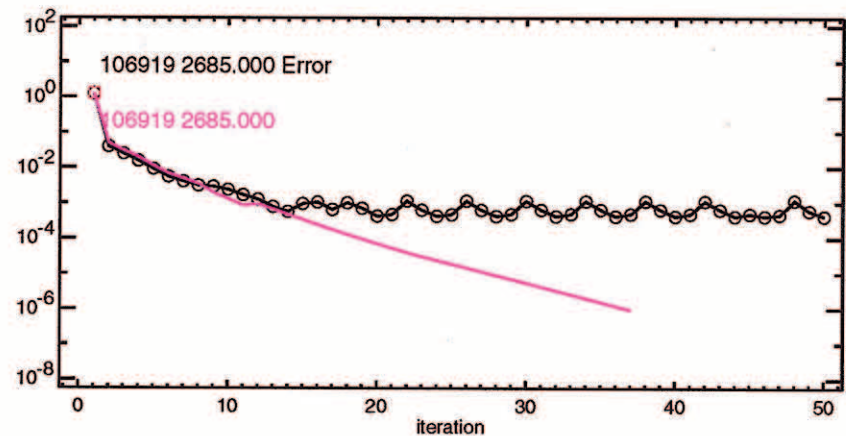
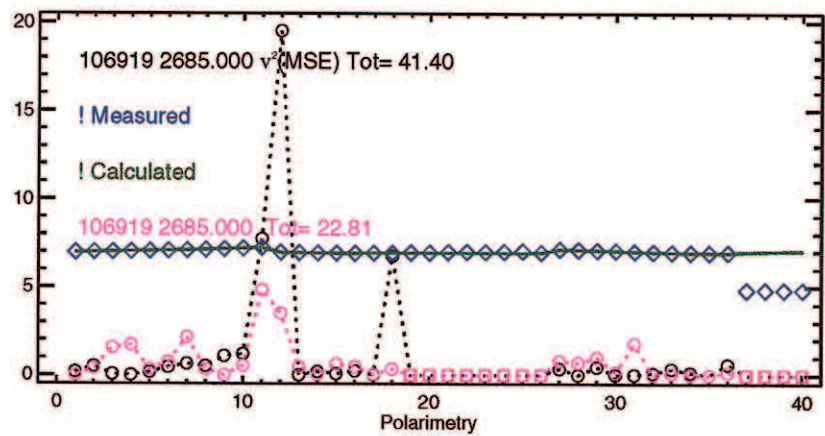
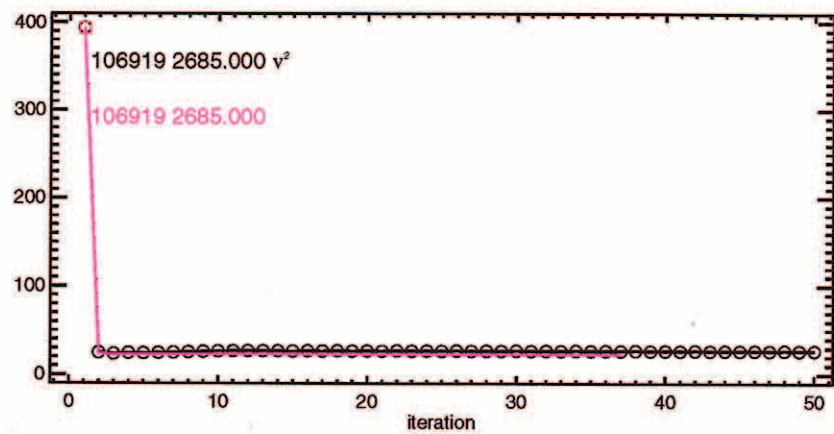
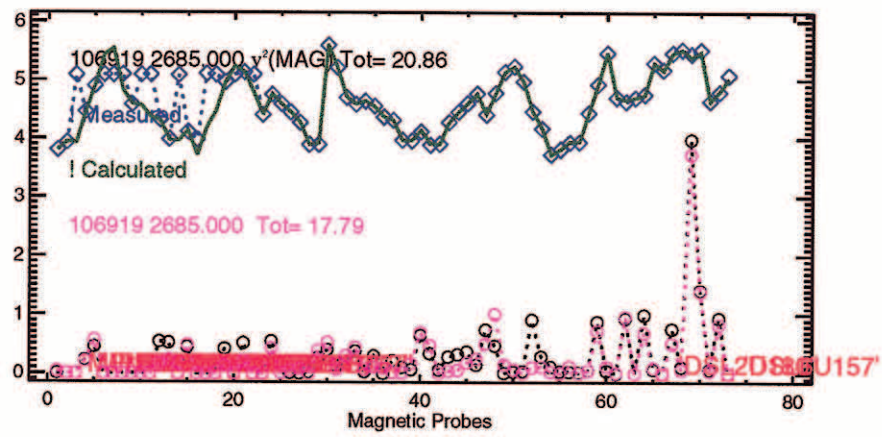


QDB/QH/EHO Shot with E_r

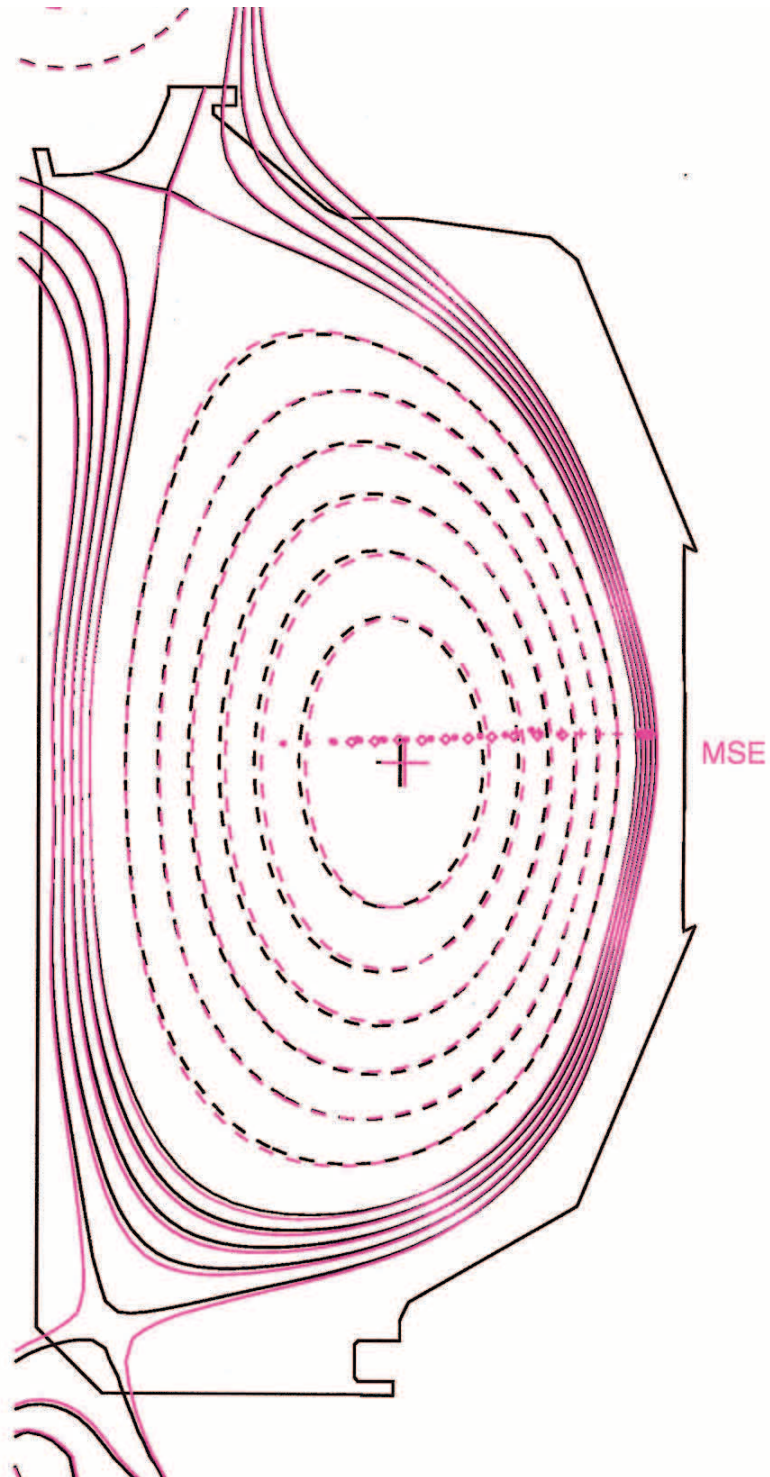






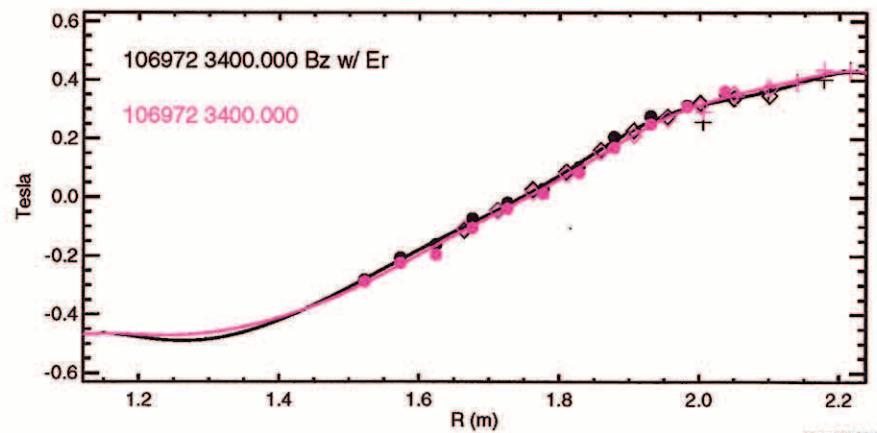
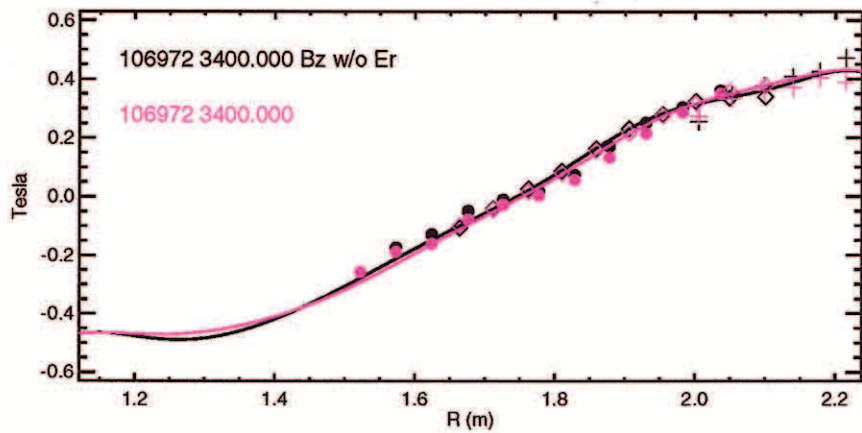
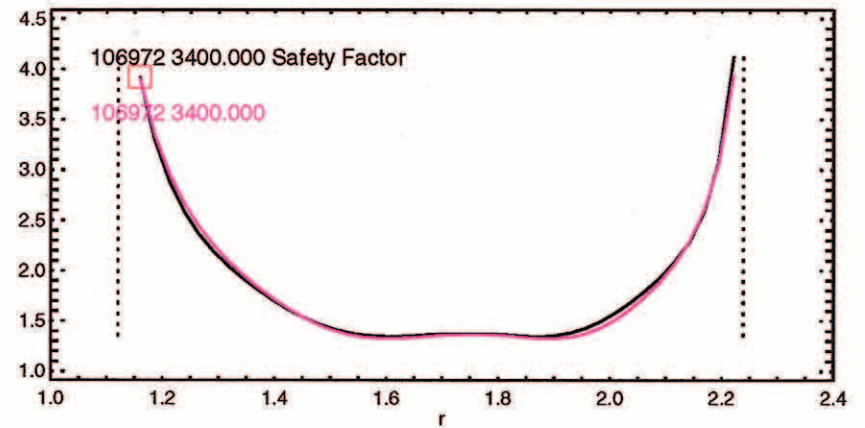
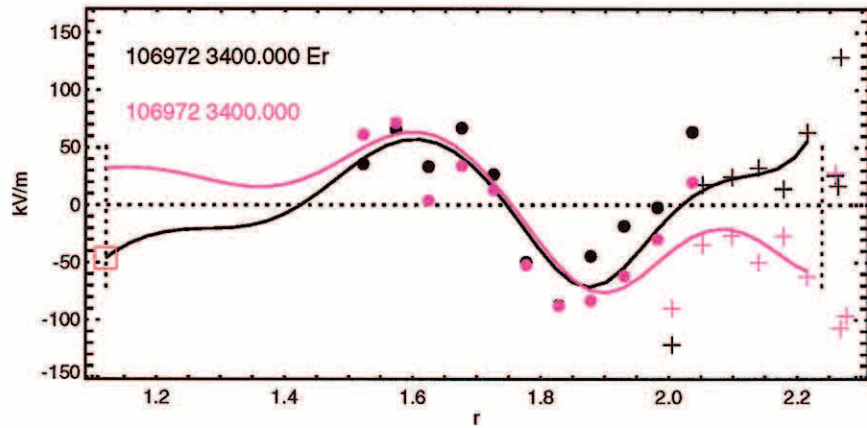
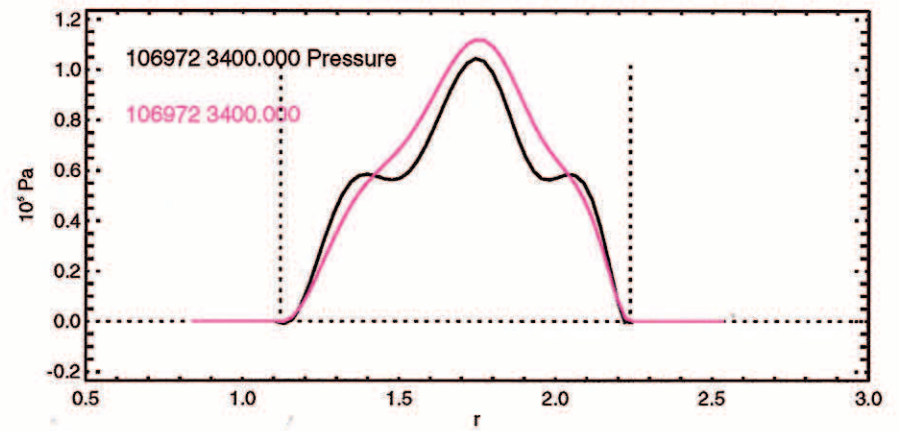
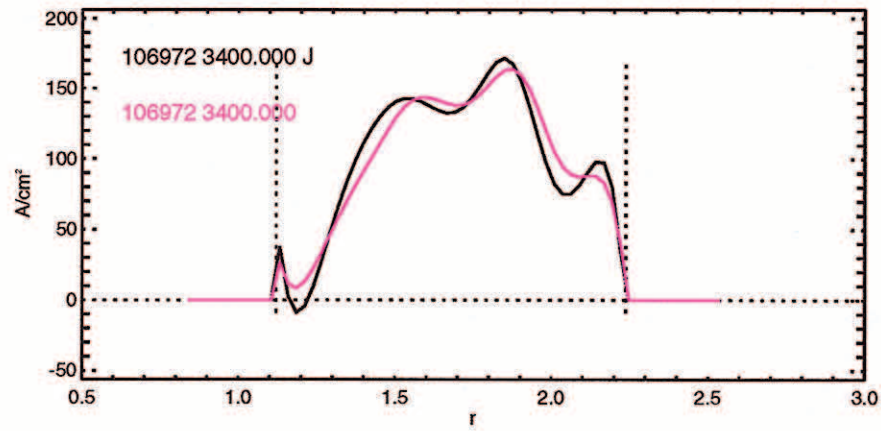


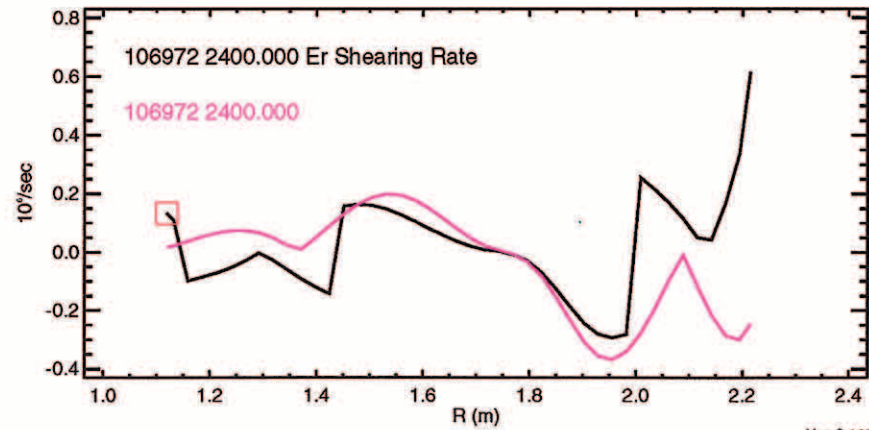
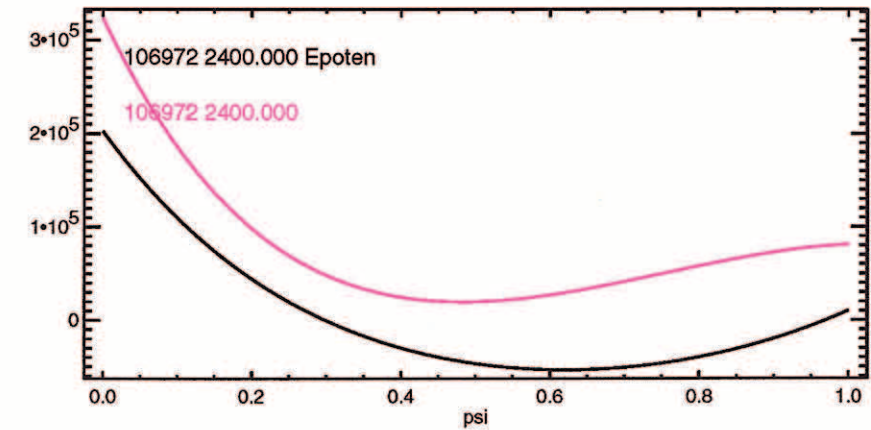
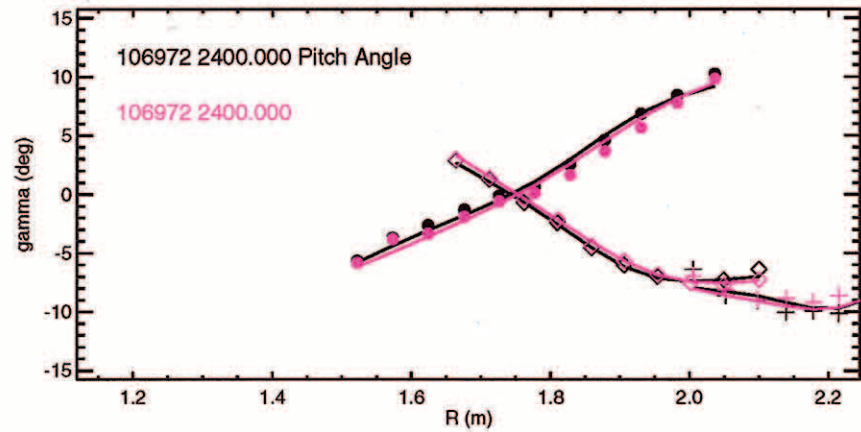
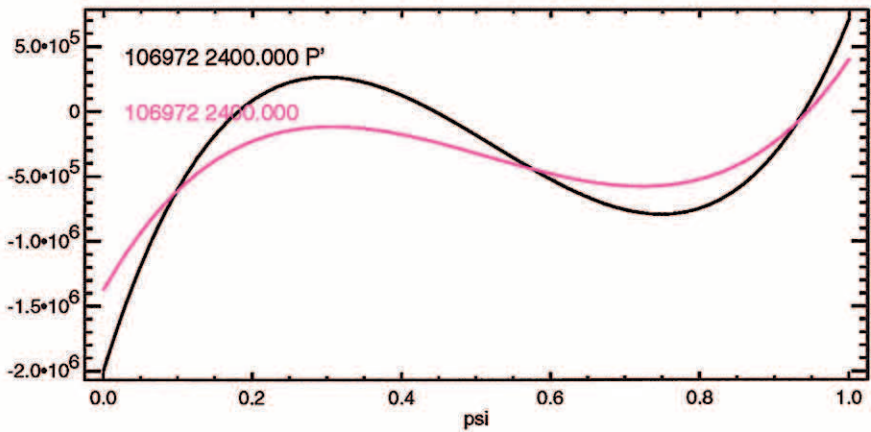
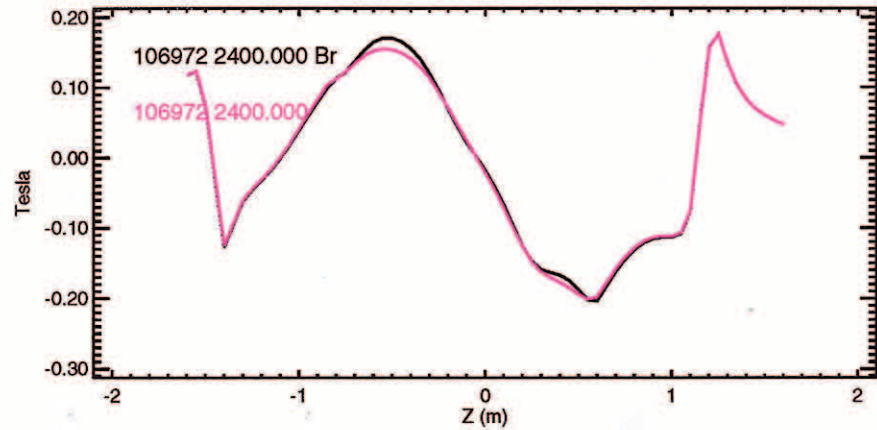
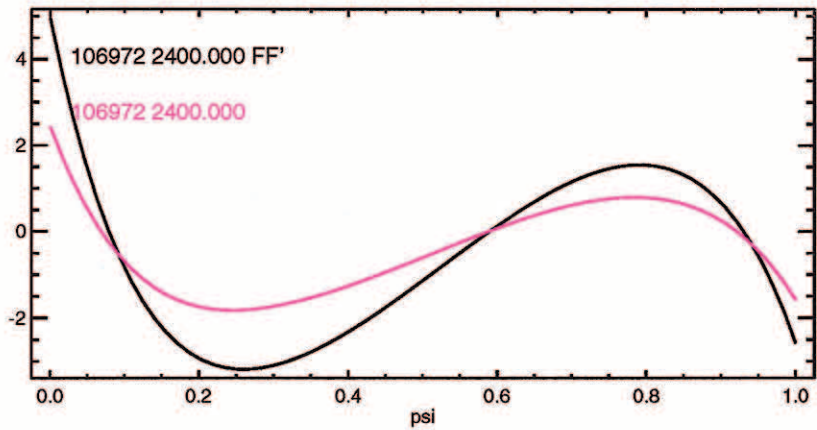
cnr**2	23.123
Rout(m)	1.689
Zout(m)	0.061
a(m)	0.567
elong	1.876
utri	0.719
ltri	0.233
indent	0.000
V (m**3)	18.916
A (m**2)	1.830
W (MJ)	1.107
betaT(%)	2.419
betaP	1.077
betaN	2.164
In	1.118
Li	0.883
error(e-4)	0.009
q1	7.419
q95	4.426
dsep(m)	0.097
Rm(m)	1.775
Zm(m)	-0.054
Rc(m)	1.738
Zc(m)	-0.034
betaPd	1.076
betaTd	2.416
Wdia(MJ)	1.105
Ipmeas(MA)	-1.272
BT(O)(T)	-2.006
Ipfit(MA)	-1.277
Rmidin(m)	1.123
Rmidout(m)	2.255
gapin(m)	0.106
gapout(m)	0.097
gaptop(m)	0.105
gapbot(m)	0.234
Zts(m)	0.754
Rvsin(m)	1.125
Zvsin(m)	1.167
Rvsout(m)	1.356
Zvsout(m)	1.348
Rsep1(m)	1.157
Zsep1(m)	-1.230
Rsep2(m)	1.282
Zsep2(m)	1.126
psib(Vs/R)	-0.087
elongm	1.607
qm	1.502
nev1(e19)	1.746
nev2(e19)	2.248
nev3(e19)	1.455
ner0(e19)	2.545
n/nc	-0.787
dRsep	0.039
qmin	1.465
rhoqmin	0.216

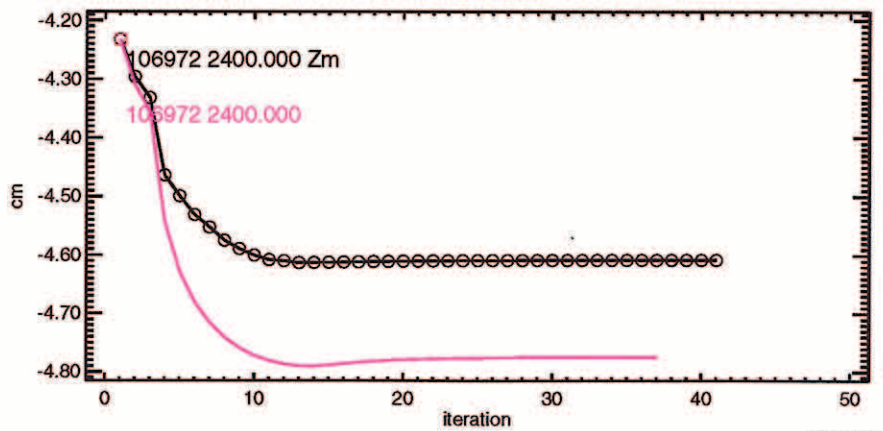
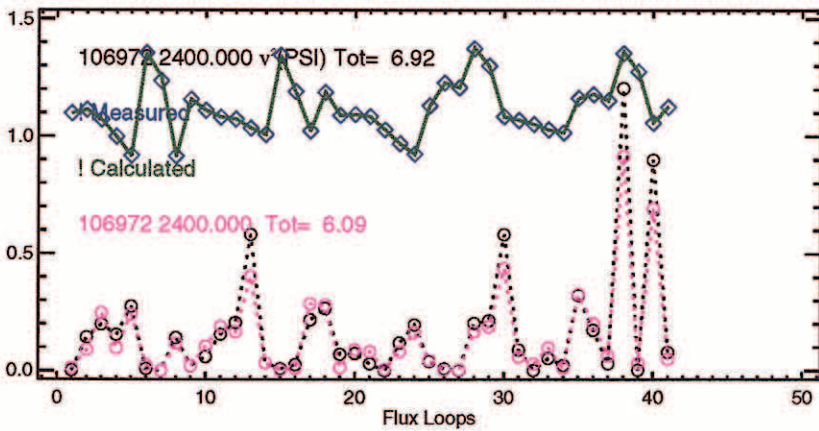
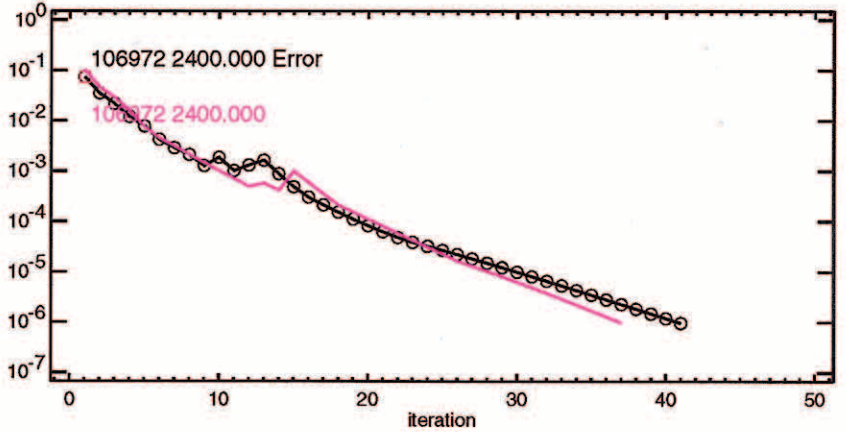
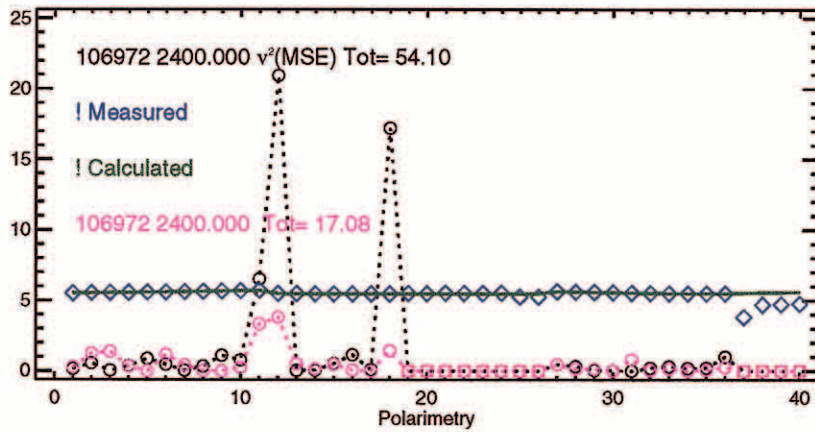
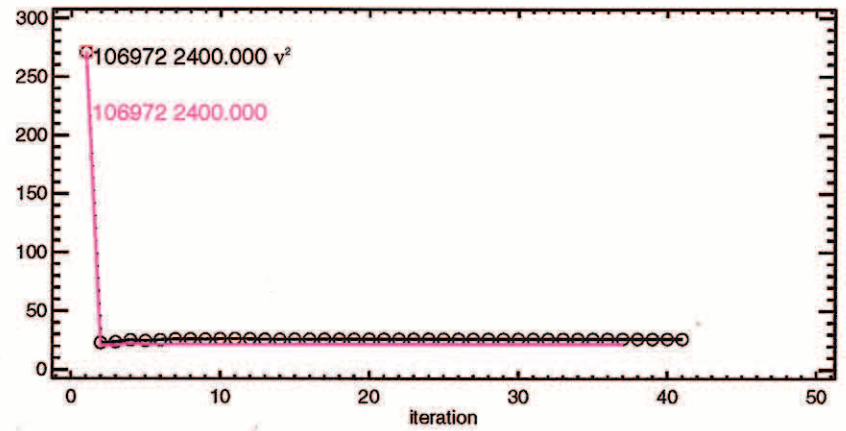
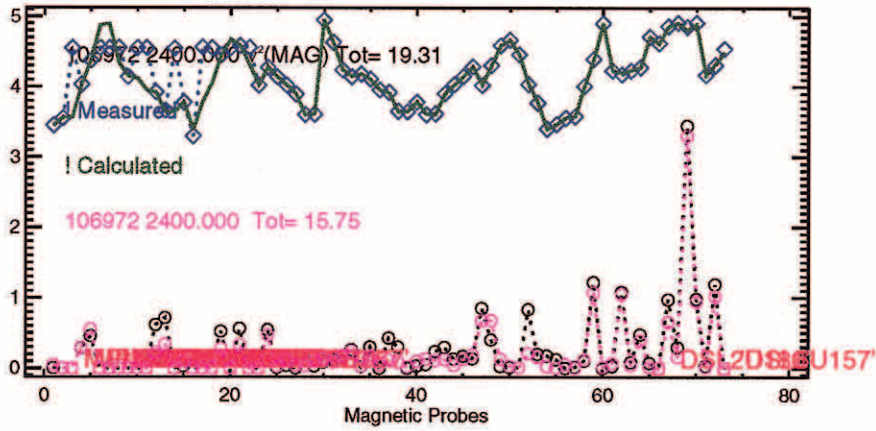


Thrust 7, Counter Injection, with E_r

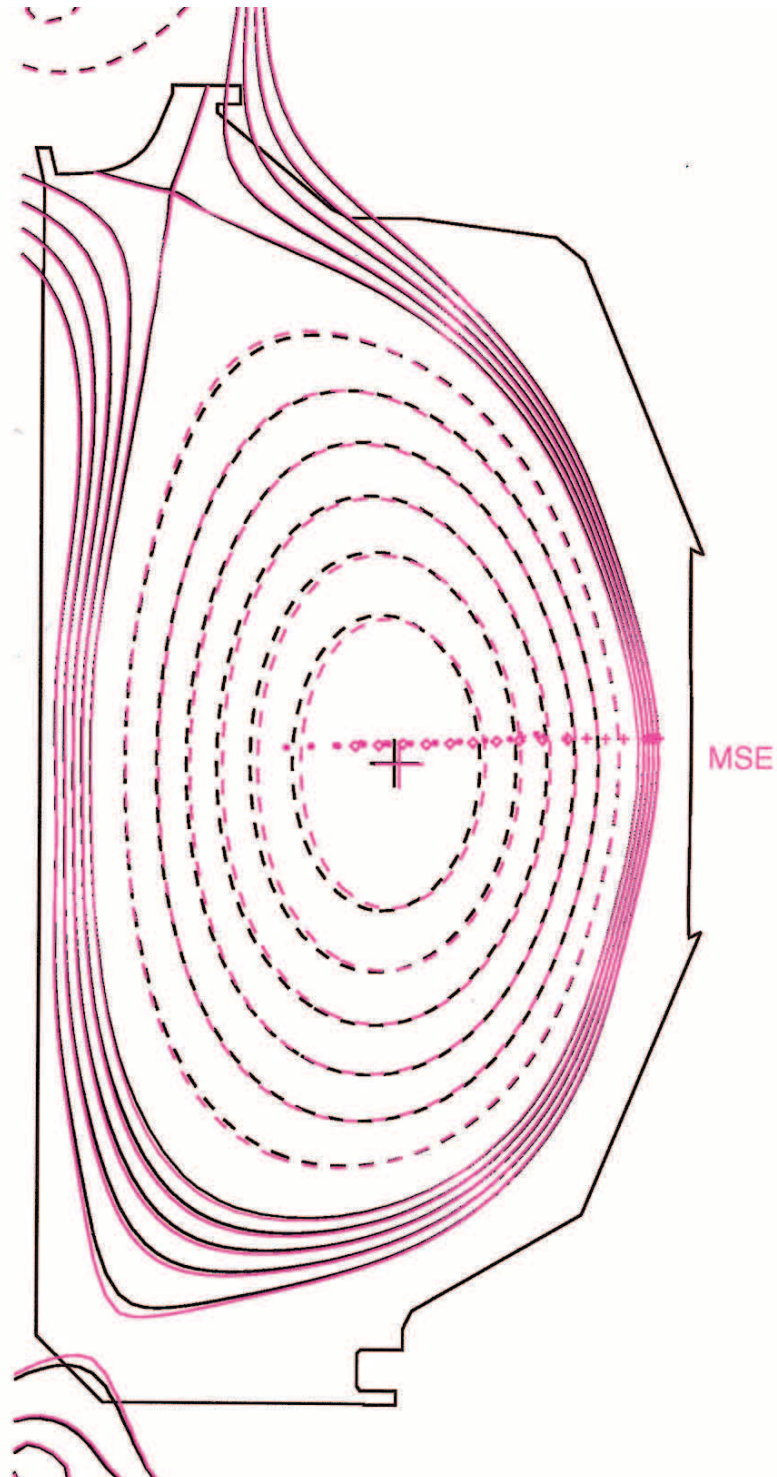






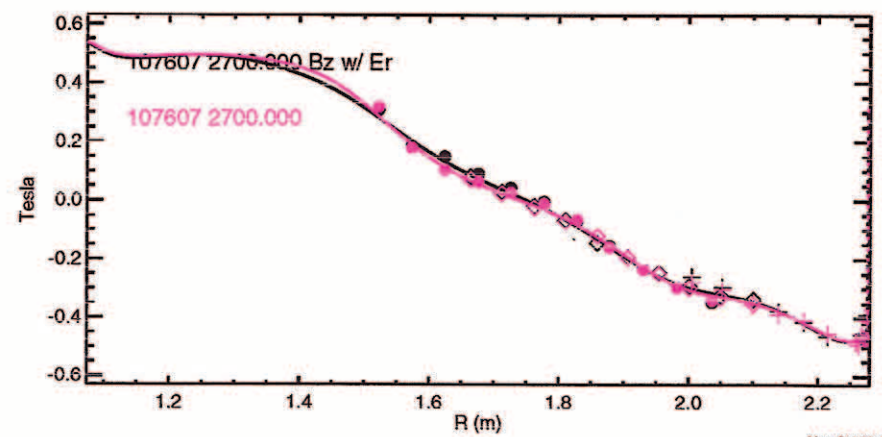
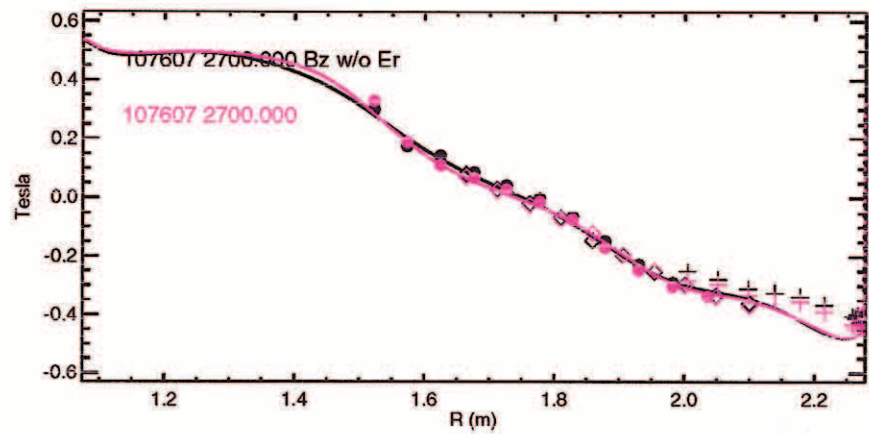
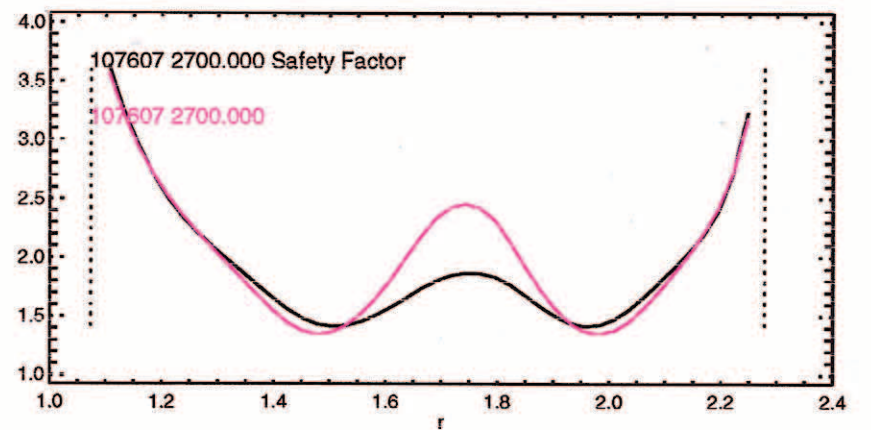
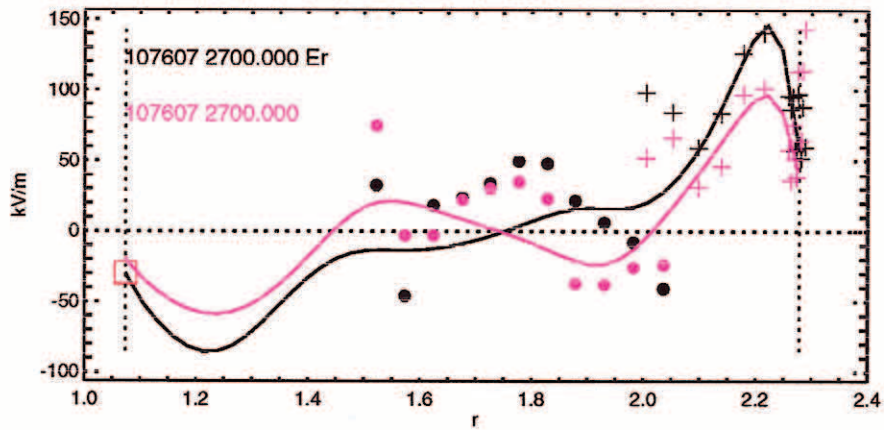
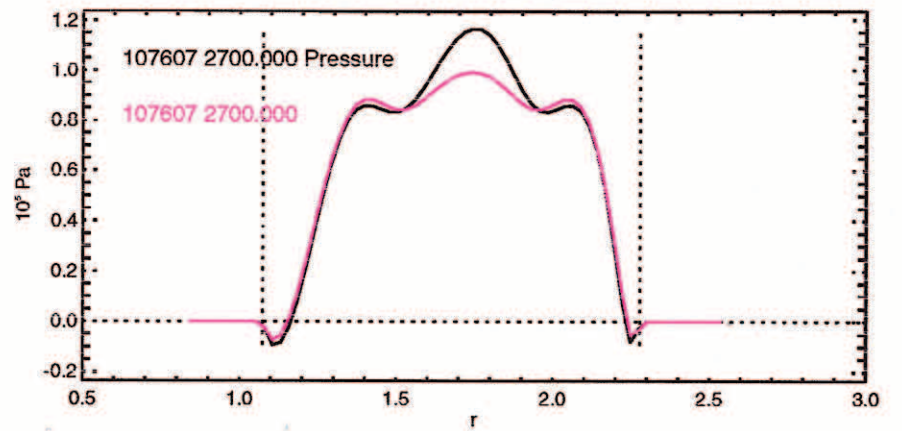
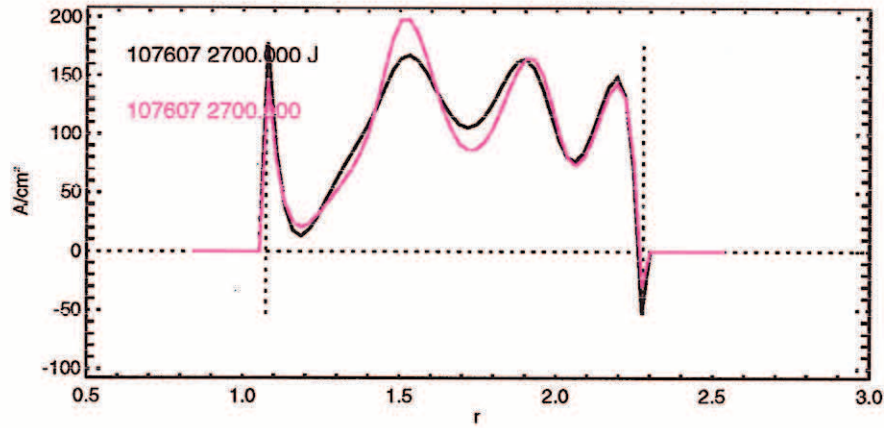


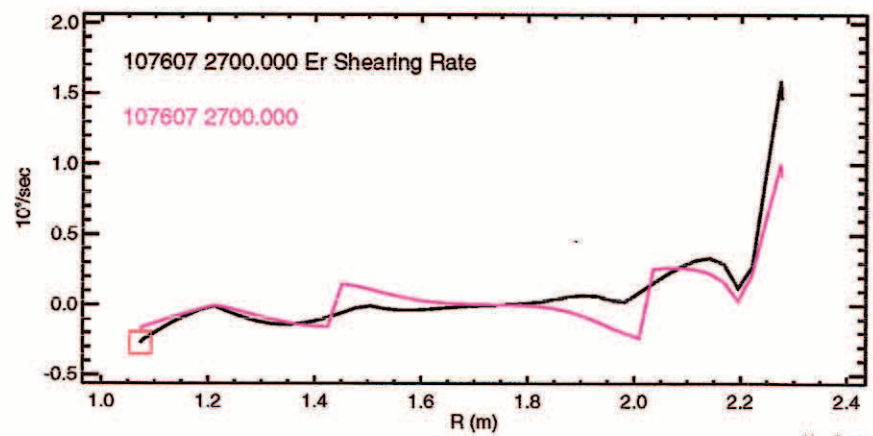
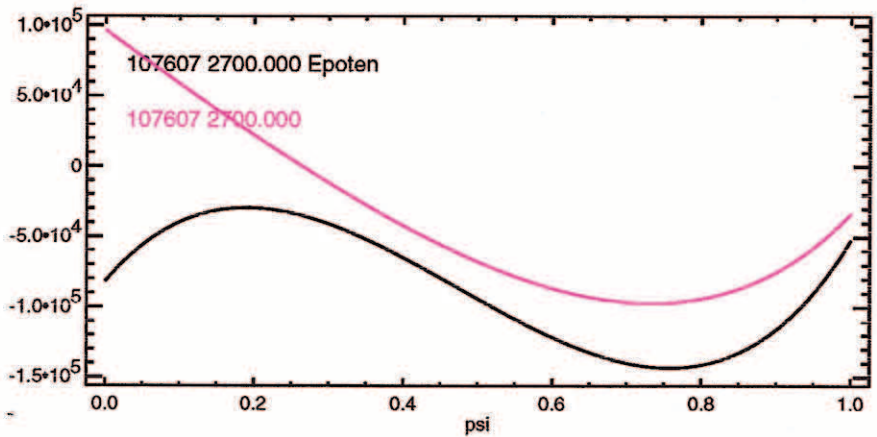
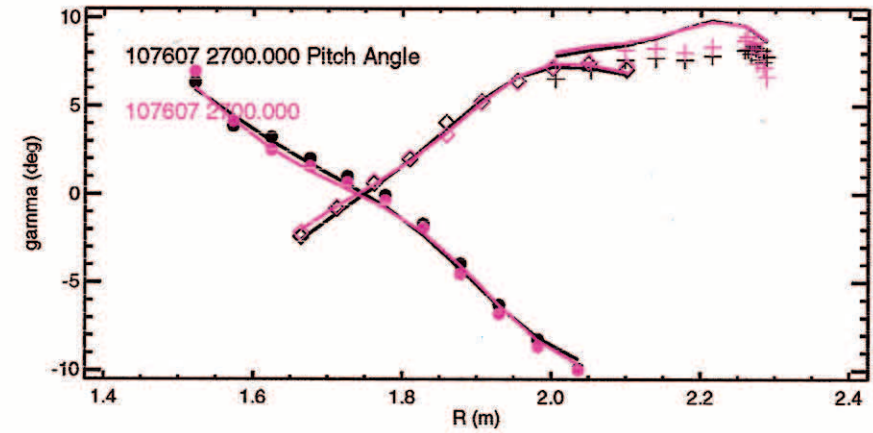
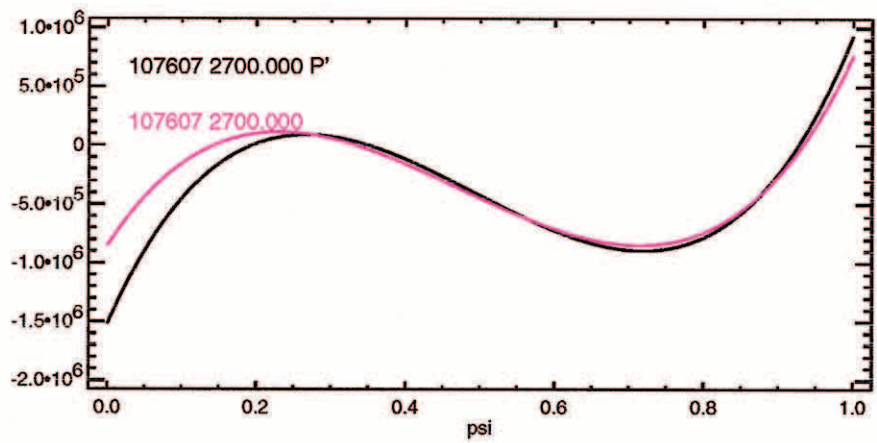
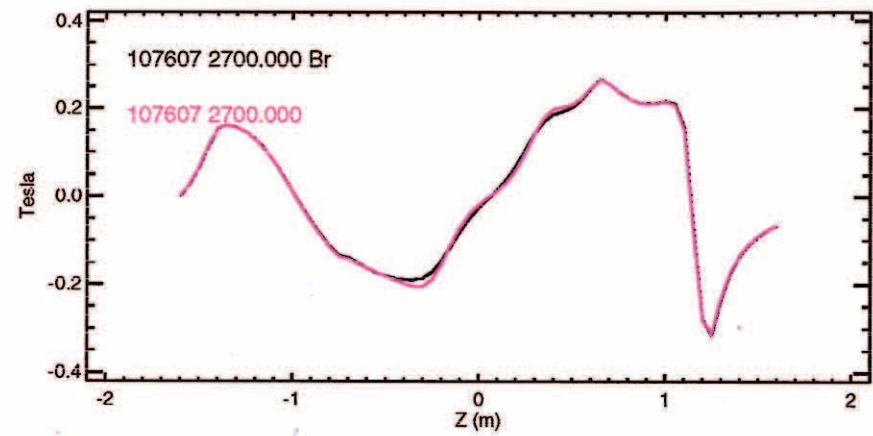
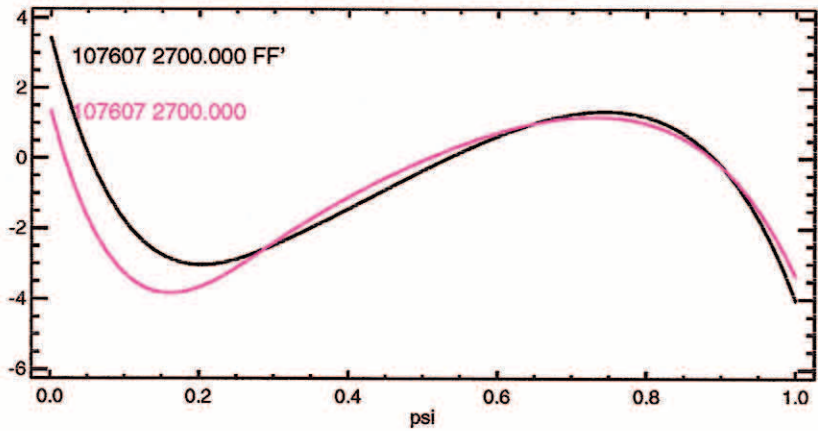
cr1(z)	21.845
Rout(m)	1.683
Zout(m)	0.067
a(m)	0.563
elong	1.878
utri	0.715
ltri	0.224
indent	0.000
V (m**3)	18.535
A (m**2)	1.800
W (MJ)	0.972
betaT(%)	2.165
betaP	0.943
betaN	1.916
ln	1.130
Li	0.886
error(e-4)	0.010
q1	7.256
q95	4.318
dsep(m)	0.105
Rm(m)	1.754
Zm(m)	-0.048
Rc(m)	1.721
Zc(m)	-0.029
betaPd	0.929
betaTd	2.133
Wdia(MJ)	0.957
Ipmeas(MA)	-1.283
BT(0)(T)	-2.000
Ipfit(MA)	-1.281
Rmidin(m)	1.121
Rmidout(m)	2.246
gapin(m)	0.105
gapout(m)	0.108
gaptop(m)	0.106
gapbot(m)	0.249
Zts(m)	0.743
Rvsin(m)	1.119
Zvsin(m)	1.166
Rvsout(m)	1.353
Zvsout(m)	1.348
Rsep1(m)	-9.990
Zsep1(m)	-9.990
Rsep2(m)	1.281
Zsep2(m)	1.124
psib(Vs/R)	-0.096
elongm	1.592
qm	1.501
nev1(e19)	1.695
nev2(e19)	2.049
nev3(e19)	1.198
ner0(e19)	2.523
n/nc	-0.805
dRsep	0.400
qmin	1.466
rhoqmin	0.216

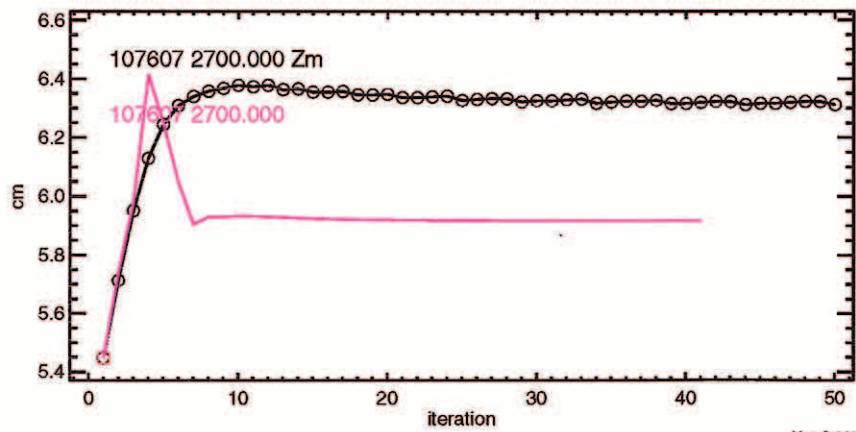
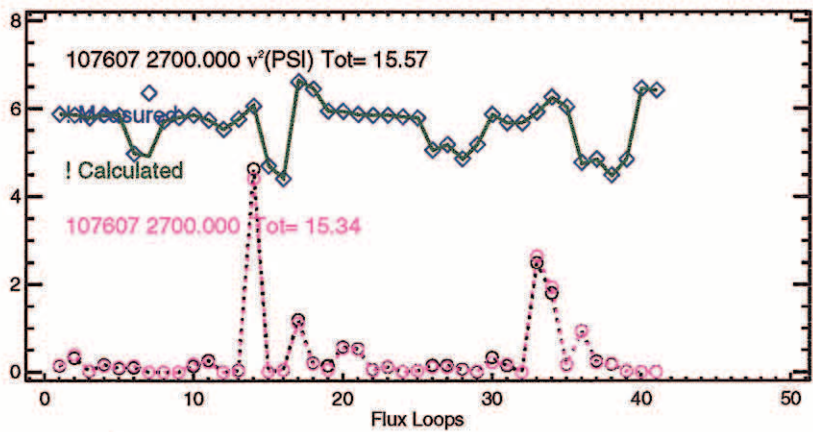
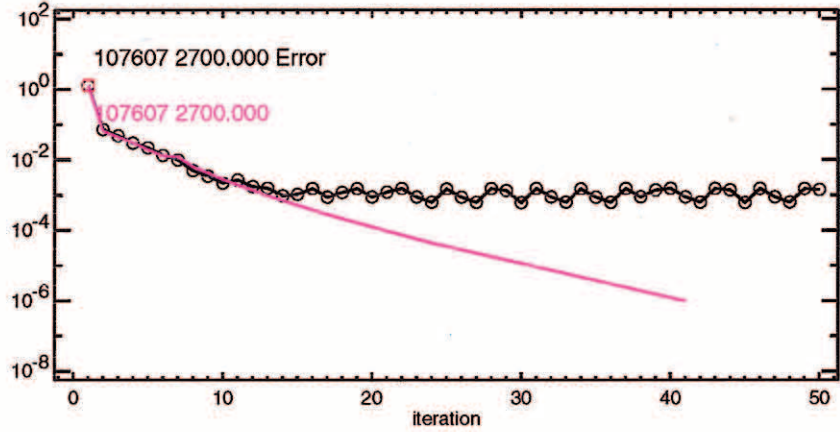
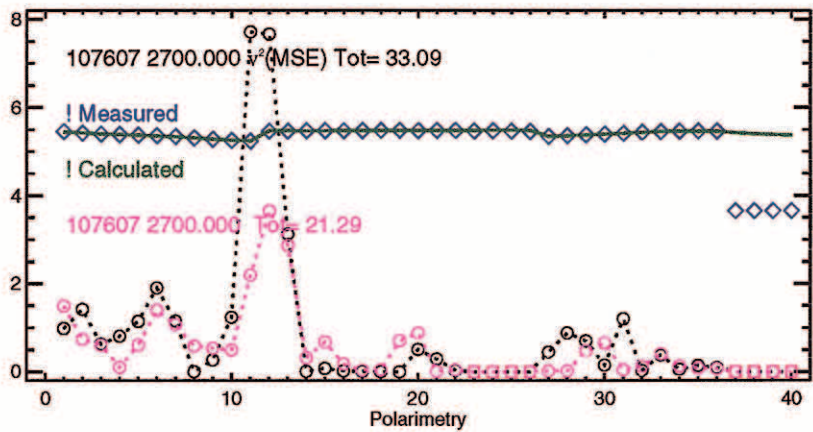
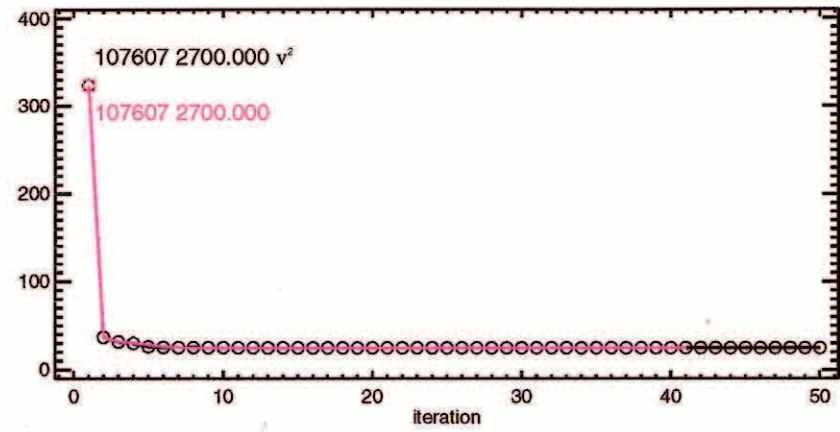
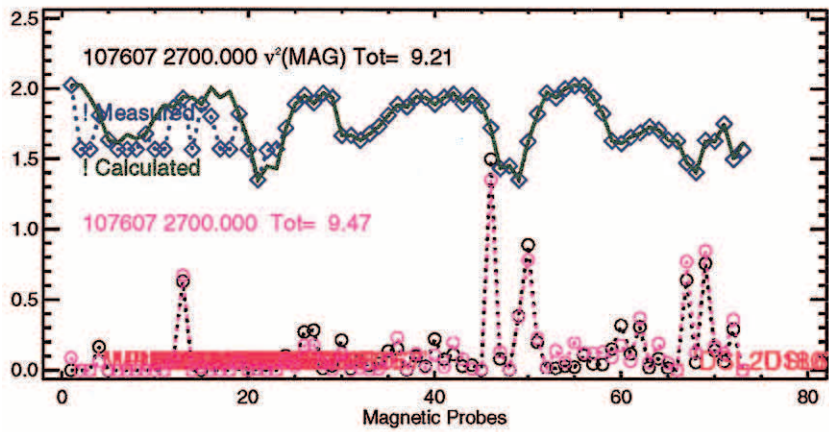


RWM Shot with E_r

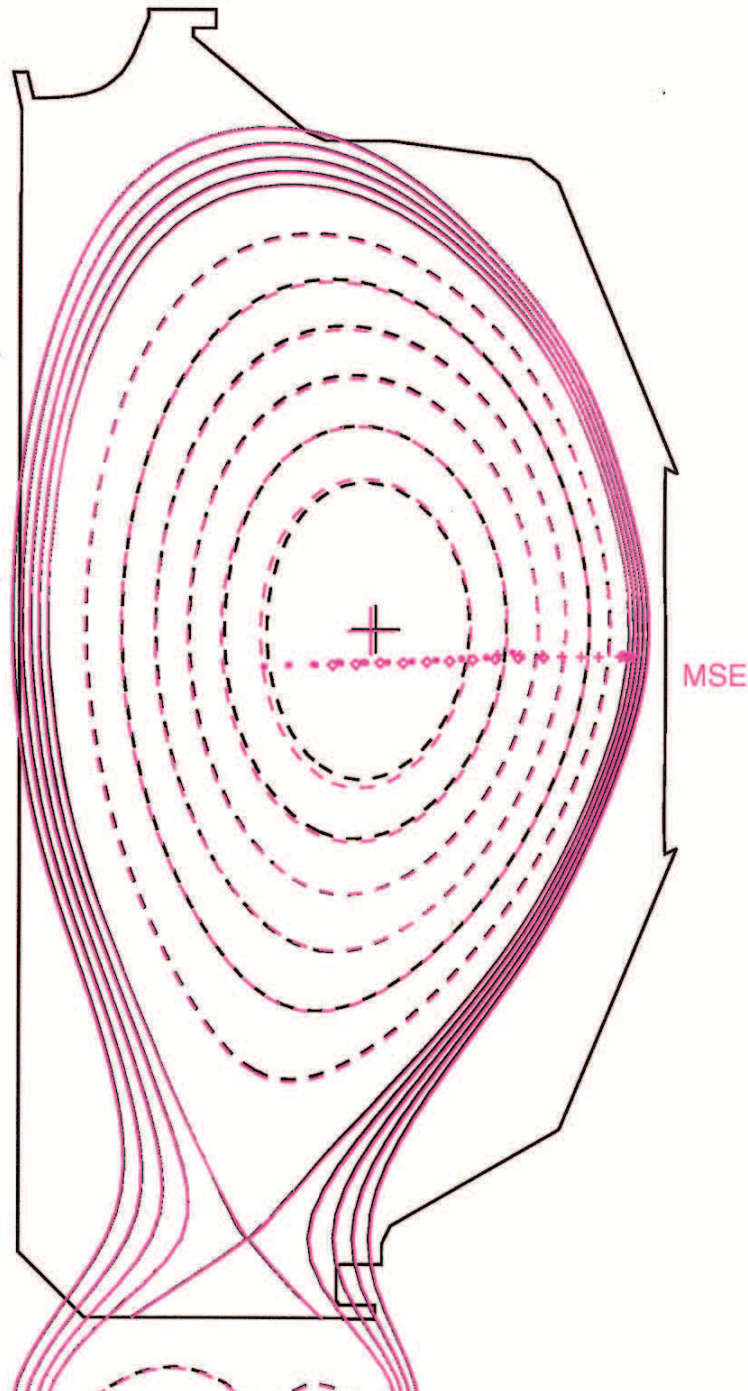






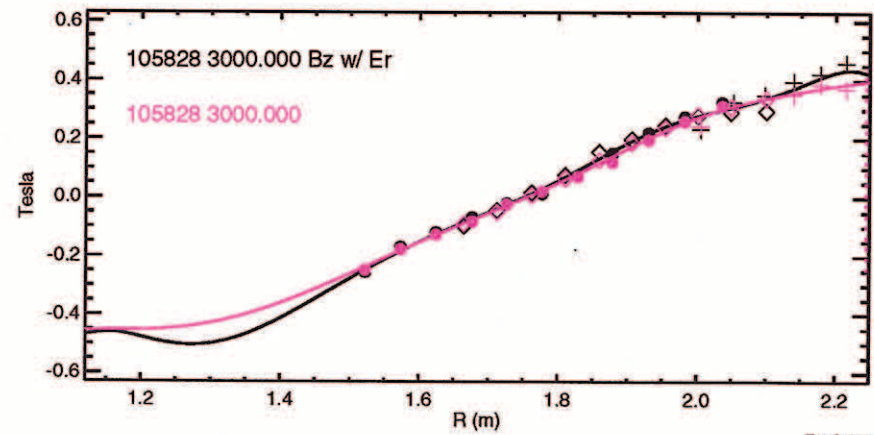
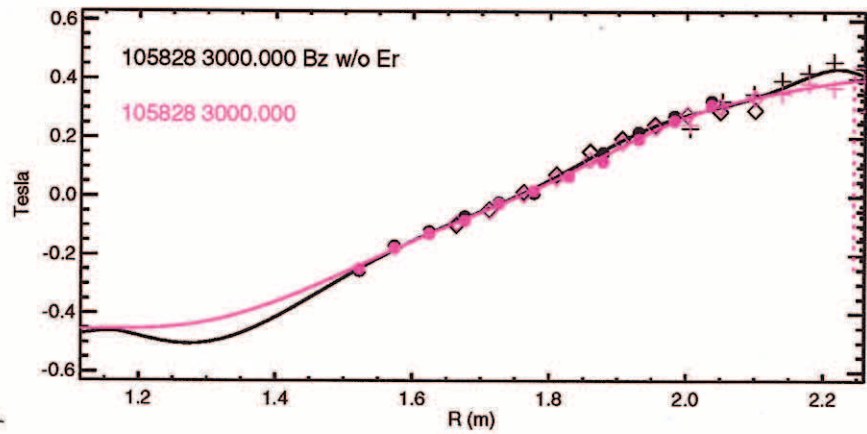
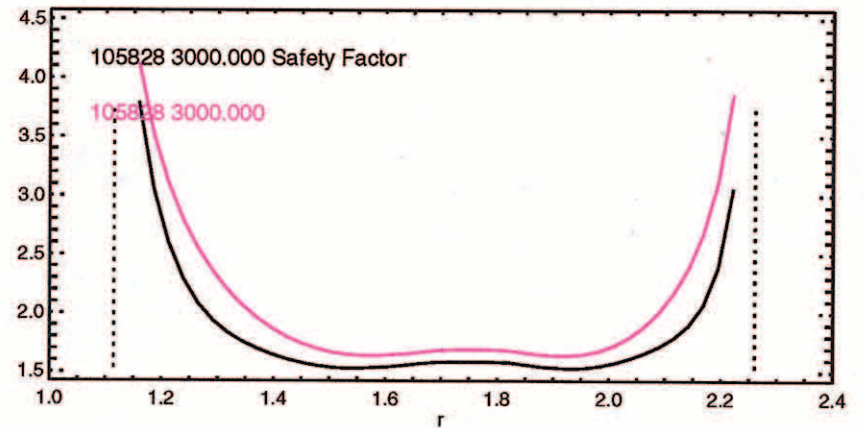
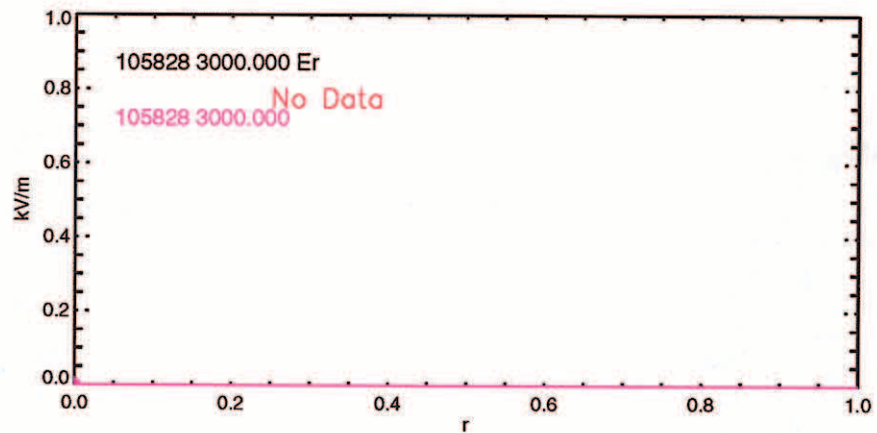
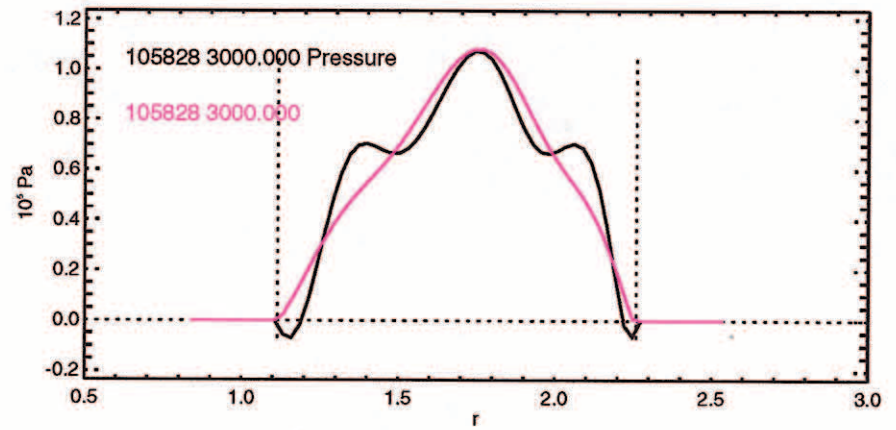
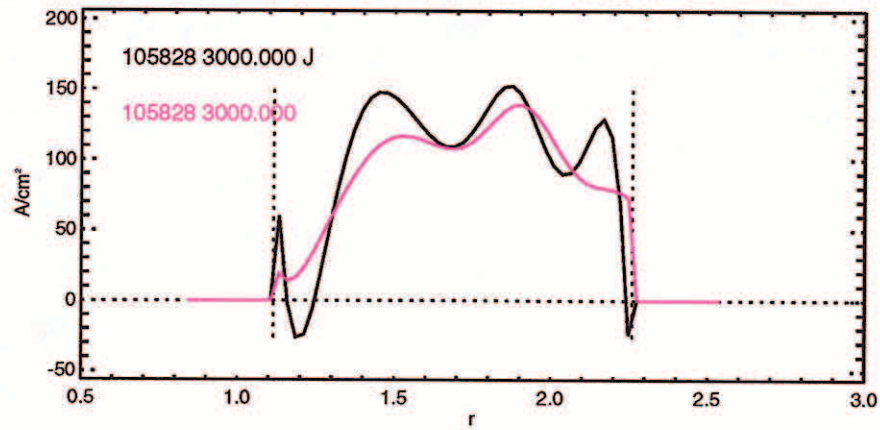


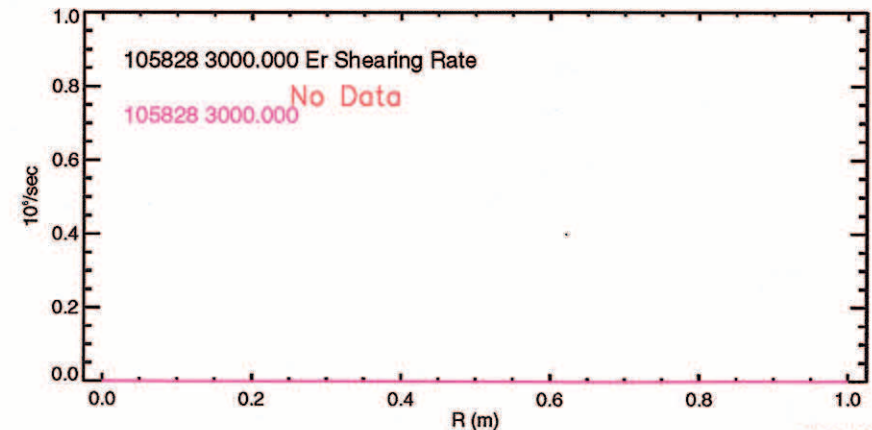
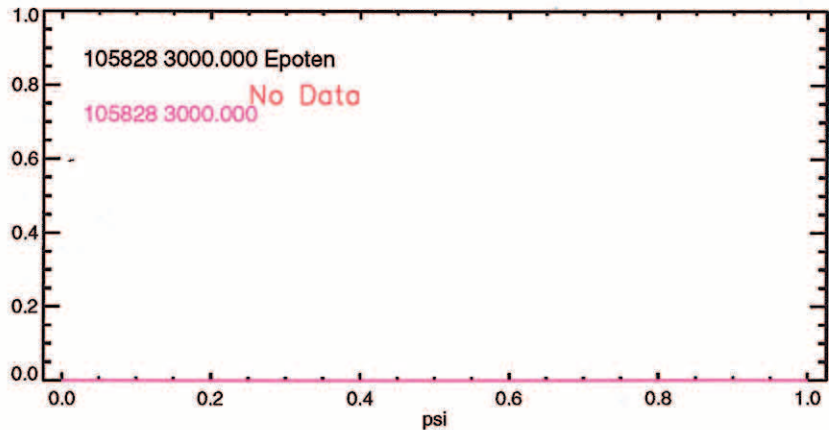
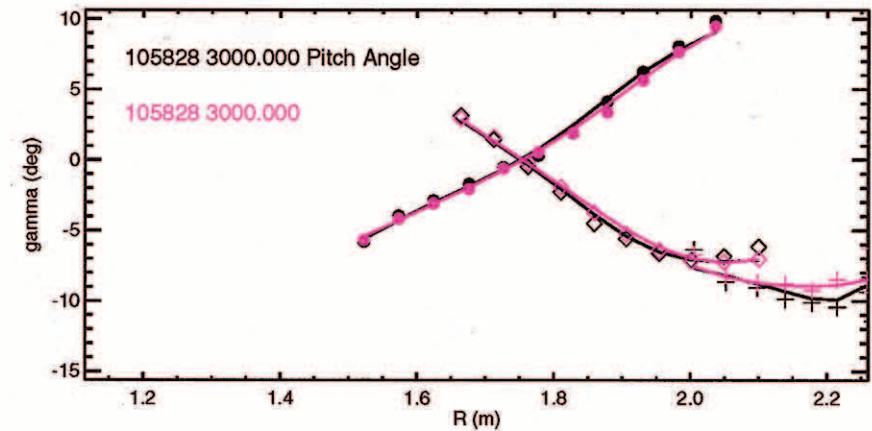
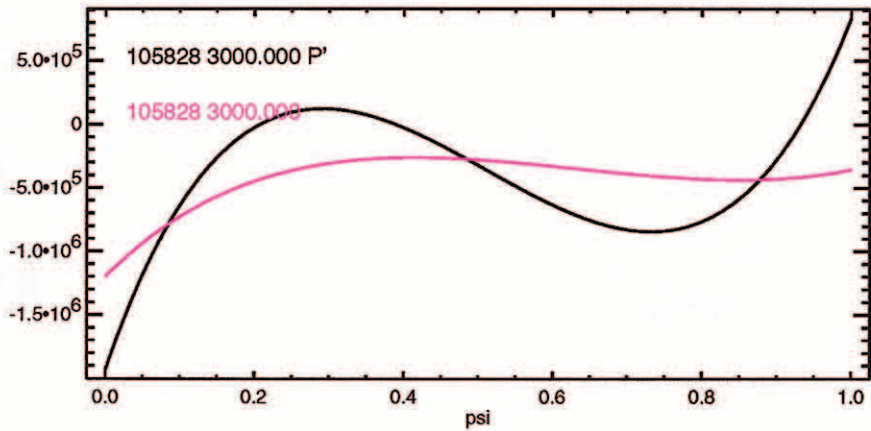
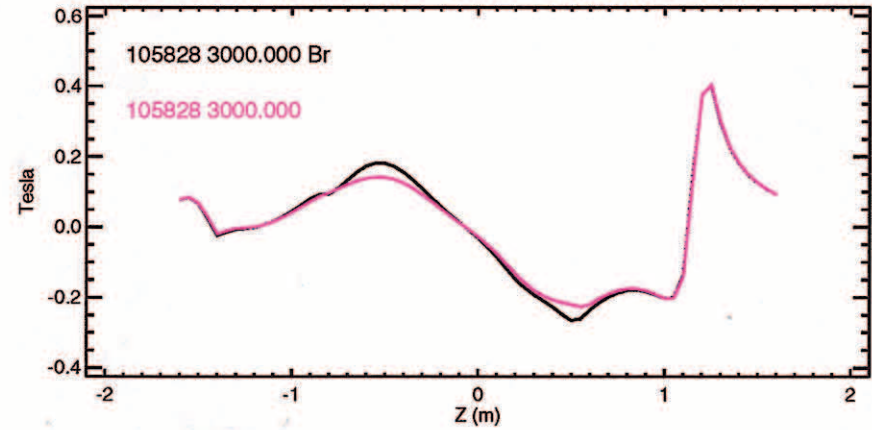
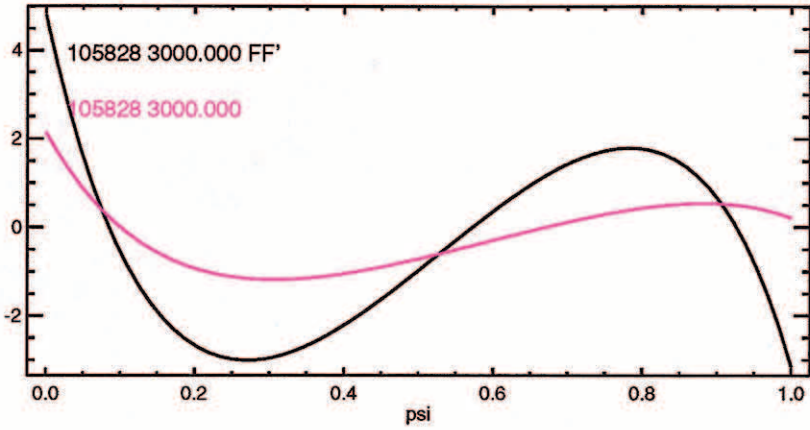
chi**2	24.868
Rout(m)	1.676
Zout(m)	-0.110
a(m)	0.603
elong	1.812
utri	0.153
ltri	0.306
indent	0.000
V (m**3)	18.888
A (m**2)	1.832
W (MJ)	1.390
betaT(%)	2.741
betaP	0.827
betaN	2.156
ln	1.271
Li	0.750
error(e-4)	0.010
q1	5.272
q95	3.652
dsep(m)	0.057
Rm(m)	1.742
Zm(m)	0.059
Rc(m)	1.709
Zc(m)	0.021
betaPd	0.919
betaTd	3.045
Wdia(MJ)	1.544
lpmeas(MA)	1.614
BT(0)(T)	-2.097
lpfit(MA)	1.626
Rmidin(m)	1.075
Rmidout(m)	2.277
gapin(m)	0.057
gapout(m)	0.074
gaptop(m)	0.323
gapbot(m)	0.163
Zts(m)	0.821
Rvsin(m)	1.250
Zvsin(m)	-1.366
Rvsout(m)	1.646
Zvsout(m)	-1.366
Rsep1(m)	1.492
Zsep1(m)	-1.203
Rsep2(m)	-9.990
Zsep2(m)	-9.990
psib(Vs/R)	0.135
elongm	1.608
qm	2.453
nev1(e19)	5.040
nev2(e19)	5.602
nev3(e19)	5.215
ner0(e19)	-2.201
n/nc	-0.425
dRsep	-0.400
qmin	1.347
rhoqmin	0.411

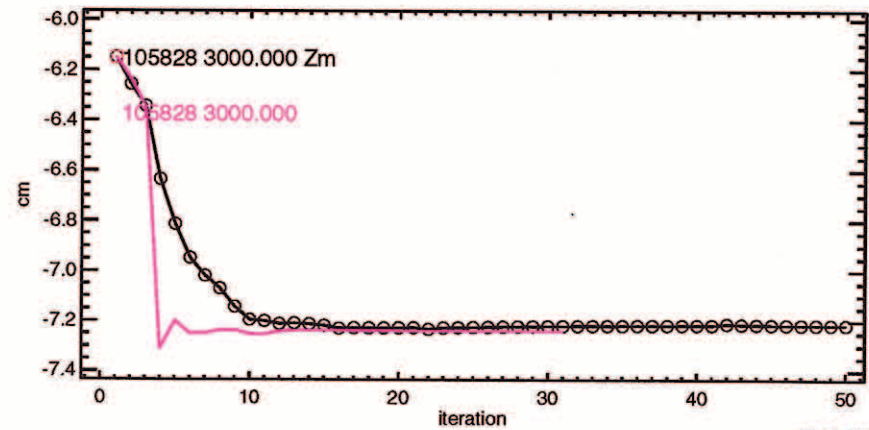
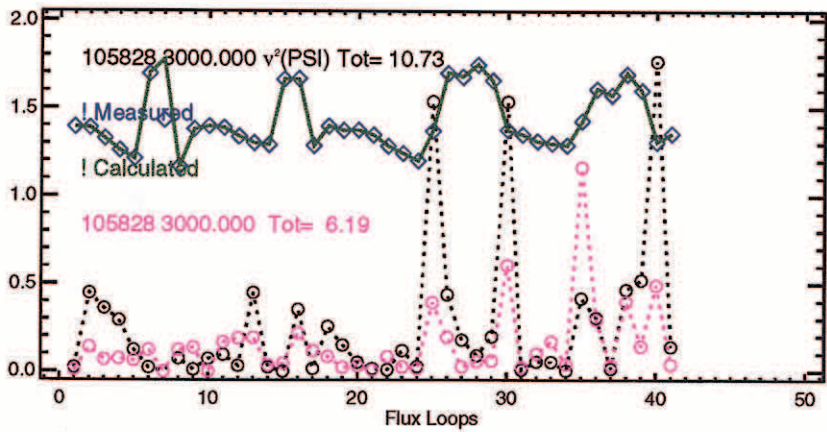
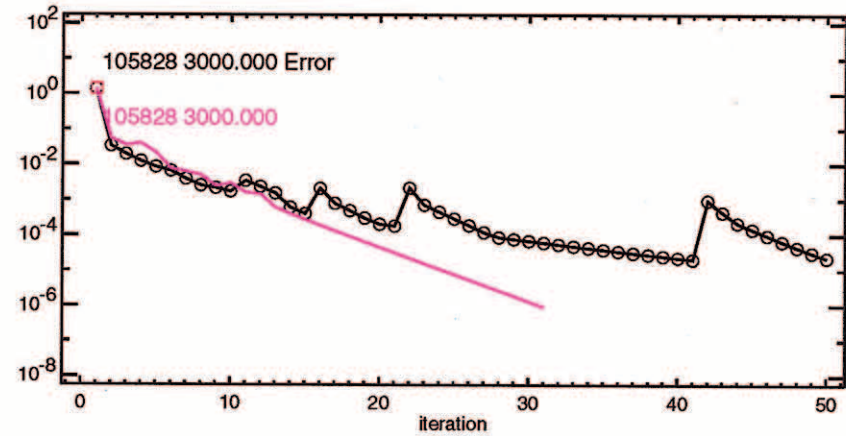
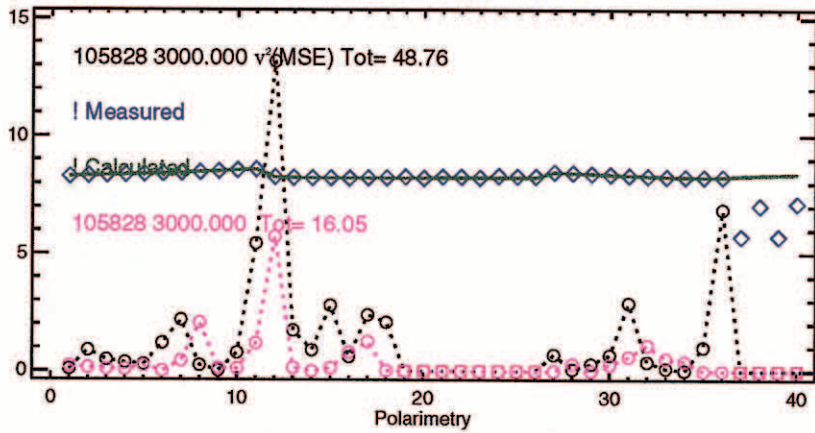
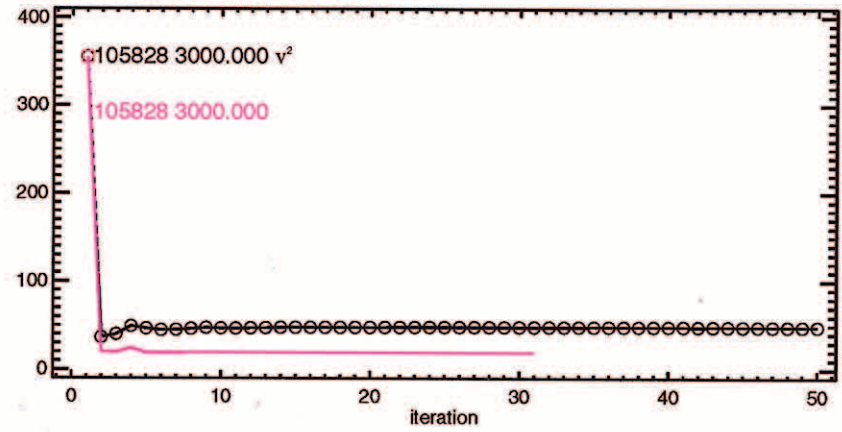
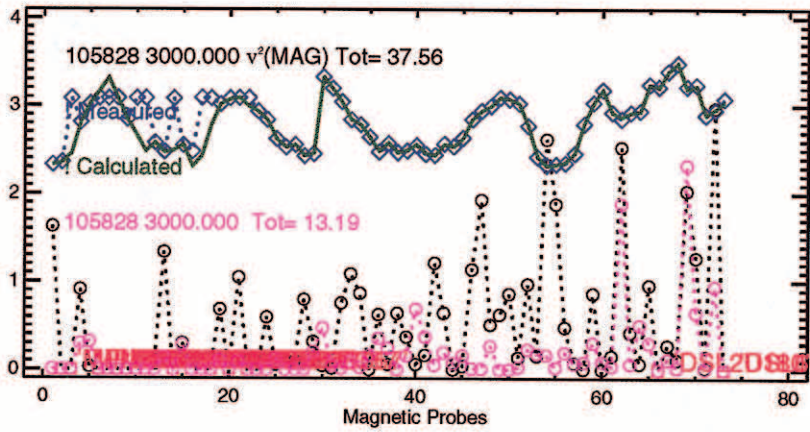


QH Mode, No E_r

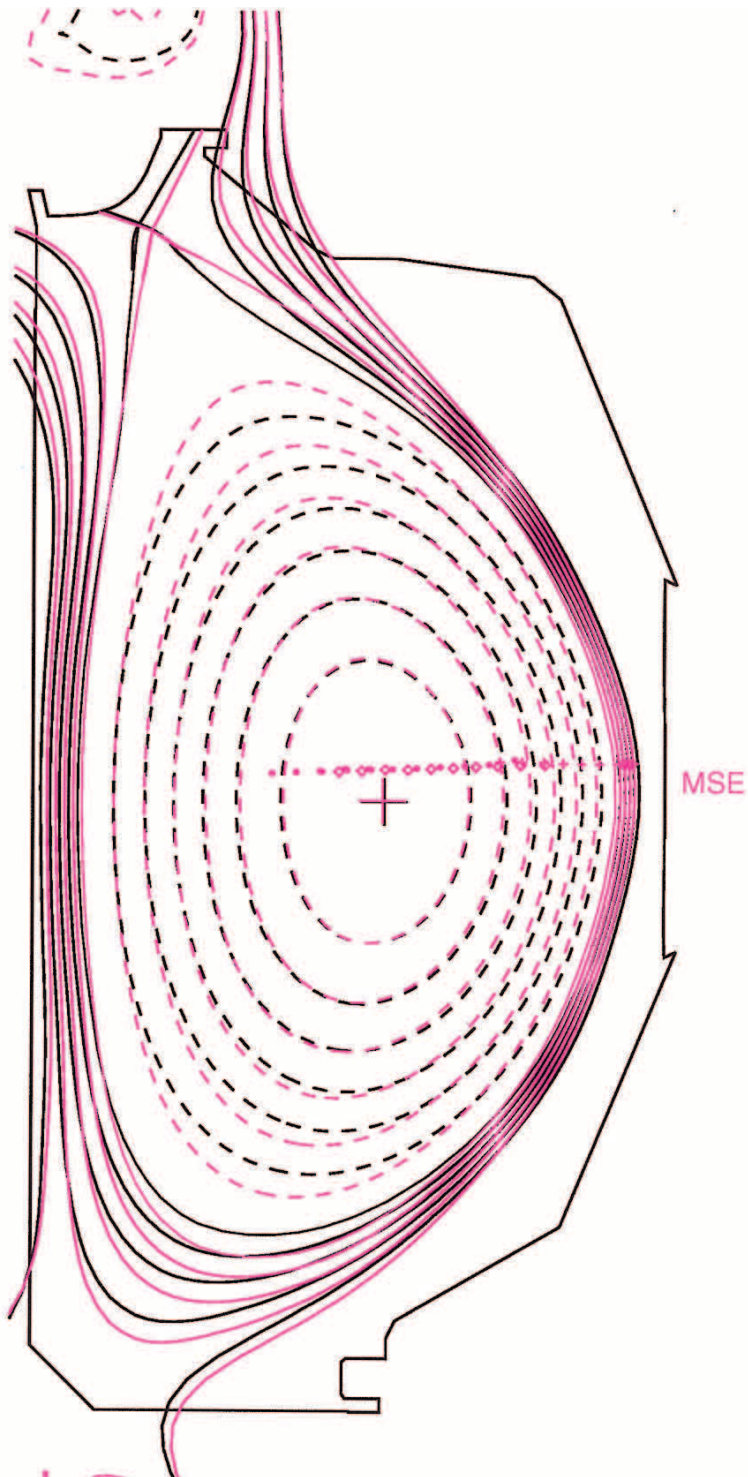








shot	103828
time	3000.0000
chi**2	19.385
Rout(m)	1.685
Zout(m)	0.046
a(m)	0.565
elong	1.922
utri	0.746
ltri	0.367
indent	0.000
V (m**3)	18.099
A (m**2)	1.776
W (MJ)	1.116
betaT(%)	2.546
betaP	1.110
betaN	2.242
In	1.136
Li	0.830
error(e-4)	0.009
q1	8.638
q95	4.604
dsep(m)	0.089
Rm(m)	1.757
Zm(m)	-0.072
Rc(m)	1.714
Zc(m)	-0.053
betaPd	1.144
betaTd	2.626
Wdia(MJ)	1.151
Ipmeas(MA)	-1.295
BT(O)(T)	-2.002
Ipfit(MA)	-1.293
Rmidin(m)	1.120
Rmidout(m)	2.244
gapin(m)	0.104
gapout(m)	0.104
gaptop(m)	0.089
gapbot(m)	0.231
Zts(m)	0.645
Rvsin(m)	1.149
Zvsin(m)	1.172
Rvsout(m)	1.368
Zvsout(m)	1.348
Rsep1(m)	1.166
Zsep1(m)	-1.345
Rsep2(m)	1.264
Zsep2(m)	1.132
psib(Vs/R)	-0.101
elongm	1.548
qm	1.693
nev1(e19)	2.442
nev2(e19)	2.669
nev3(e19)	1.968
ner0(e19)	3.540
n/nc	-0.629
dRsep	0.035
qmin	1.640
rhoqmin	0.294



Conclusions

- EFITs using the tangent-offset model consistently:
 - Demonstrate considerably lower χ_{mse}
 - Predict lower E_r (when present)
 - Demonstrate similar or lower χ_{mag} and χ_{psi}
 - Predict small differences in the location of the
 - The magnetic axis (± 1 cm)
 - The plasma boundary (± 1 cm)
- than those using the tangent-slope model



Conclusions (Con't)

- Only the calibration coefficients for the edge array are modified
- Elimination of the systematic error introduced by the tangent-slope model is most evident in the reduction in E_r

